JCI insight

Fibroblast deletion of ROCK2 attenuates cardiac hypertrophy, fibrosis, and diastolic dysfunction

Toru Shimizu, … , John Blair, James K. Liao

JCI Insight. 2017;2(13):e93187. https://doi.org/10.1172/jci.insight.93187.

Research Article Cardiology

Although left ventricular (LV) diastolic dysfunction is often associated with hypertension, little is known regarding its underlying pathophysiological mechanism. Here, we show that the actin cytoskeletal regulator, Rho-associated coiled-coil containing kinase-2 (ROCK2), is a critical mediator of LV diastolic dysfunction. In response to angiotensin II (Ang II), mutant mice with fibroblast-specific deletion of ROCK2 ($ROCK2^{Postn-/-}$) developed less LV wall thickness and fibrosis, along with improved isovolumetric relaxation. This corresponded with decreased connective tissue growth factor (CTGF) and fibroblast growth factor–2 (FGF2) expression in the hearts of $ROCK2^{Postn-/-}$ mice. Indeed, knockdown of ROCK2 in cardiac fibroblasts leads to decreased expression of CTGF and secretion of FGF2, and cardiomyocytes incubated with conditioned media from ROCK2-knockdown cardiac fibroblasts exhibited less hypertrophic response. In contrast, mutant mice with elevated fibroblast ROCK activity exhibited enhanced Ang II–stimulated cardiac hypertrophy and fibrosis. Clinically, higher leukocyte ROCK2 activity was observed in patients with diastolic dysfunction compared with age- and sex-matched controls, and correlated with higher grades of diastolic dysfunction by echocardiography. These findings indicate that fibroblast ROCK2 is necessary to cause cardiac hypertrophy and fibrosis through the induction CTGF and FGF2, and they suggest that targeting ROCK2 may have therapeutic benefits in patients with LV diastolic dysfunction.

JCI insight

RESEARCH ARTICLE

Fibroblast deletion of ROCK2 attenuates cardiac hypertrophy, fibrosis, and diastolic dysfunction

Toru Shimizu, Nikhil Narang, Phetcharat Chen, Brian Yu, Maura Knapp, Jyothi Janardanan, John Blair, and James K. Liao

Section of Cardiology, Department of Medicine, University of Chicago, Chicago, Illinois, USA.

Although left ventricular (LV) diastolic dysfunction is often associated with hypertension, little is known regarding its underlying pathophysiological mechanism. Here, we show that the actin cytoskeletal regulator, Rho-associated coiled-coil containing kinase-2 (ROCK2), is a critical mediator of LV diastolic dysfunction. In response to angiotensin II (Ang II), mutant mice with fibroblast-specific deletion of ROCK2 (ROCK2$^{Postn-/-}$) developed less LV wall thickness and fibrosis, along with improved isovolumetric relaxation. This corresponded with decreased connective tissue growth factor (CTGF) and fibroblast growth factor–2 (FGF2) expression in the hearts of ROCK2$^{Postn-/-}$ mice. Indeed, knockdown of ROCK2 in cardiac fibroblasts leads to decreased expression of CTGF and secretion of FGF2, and cardiomyocytes incubated with conditioned media from ROCK2-knockdown cardiac fibroblasts exhibited less hypertrophic response. In contrast, mutant mice with elevated fibroblast ROCK activity exhibited enhanced Ang II–stimulated cardiac hypertrophy and fibrosis. Clinically, higher leukocyte ROCK2 activity was observed in patients with diastolic dysfunction compared with age- and sex-matched controls, and correlated with higher grades of diastolic dysfunction by echocardiography. These findings indicate that fibroblast ROCK2 is necessary to cause cardiac hypertrophy and fibrosis through the induction CTGF and FGF2, and they suggest that targeting ROCK2 may have therapeutic benefits in patients with LV diastolic dysfunction.

Introduction

Heart failure (HF) is the most common reason for hospitalization in people over the age of 65 years, and it accounts for more than 1 million admissions and $23 billion annually in the US (1, 2). A great proportion of HF is due to left ventricular (LV) diastolic dysfunction (3). The incidence of LV diastolic dysfunction and the proportion of hospitalized HF patients who have LV diastolic dysfunction appears to be rising (3–5). Whereas effective medical and surgical treatments for HF with reduced LV function are available, such as angiotensin (Ang) converting enzyme inhibitors (6), cardiac transplantation (7), and LV assist devices (8), the treatment for LV diastolic dysfunction is more limited (9). This is due, in part, to our lack of understanding regarding the pathophysiological mechanisms underlying LV diastolic dysfunction, which clinically is characterized by cardiac hypertrophy, remodeling, and fibrosis (9).

The Rho-associated coiled-coil containing kinases (ROCKs) are members of the serine/threonine protein kinase family, which mediate the downstream effects of the small GTP–binding protein RhoA on the actin cytoskeleton (10–12). The Rho/ROCK pathway has been implicated in a variety of cardiovascular diseases such as hypertension, atherosclerosis, and ischemic stroke (10–12). Currently, there are two isoforms of ROCK, ROCK1 and ROCK2, with ROCK2 playing a greater role in the myocardial hypertrophic response (13–15). Although cardiomyocytes have been widely studied for their roles in the pathogenesis of cardiac disease, including cardiac hypertrophy and fibrosis, there is increasing evidence that cardiac fibroblasts (CFs), the most abundant cell type in the mammalian heart, could also play an important role in mediating cardiac hypertrophy and remodeling (16–18). However, the role of ROCK2 in CFs in mediating cardiac hypertrophy and remodeling is not known, but it could be an important pathophysiological mechanism underlying LV diastolic dysfunction. Using mutant mice with loss- and gain-of-function of ROCK2 in activated fibroblasts, we sought to determine whether CF ROCK2 is necessary and sufficient to promote cardiac hypertrophy, fibrosis, and diastolic dysfunction and, if so, to determine the downstream mechanisms involved.

Conflict of interest: The authors have declared that no conflict of interest exists.

Submitted: February 3, 2017
Accepted: May 25, 2017
Published: July 6, 2017

Reference information:
JCI Insight. 2017;2(14):e93187. https://doi.org/10.1172/jci.insight.93187.

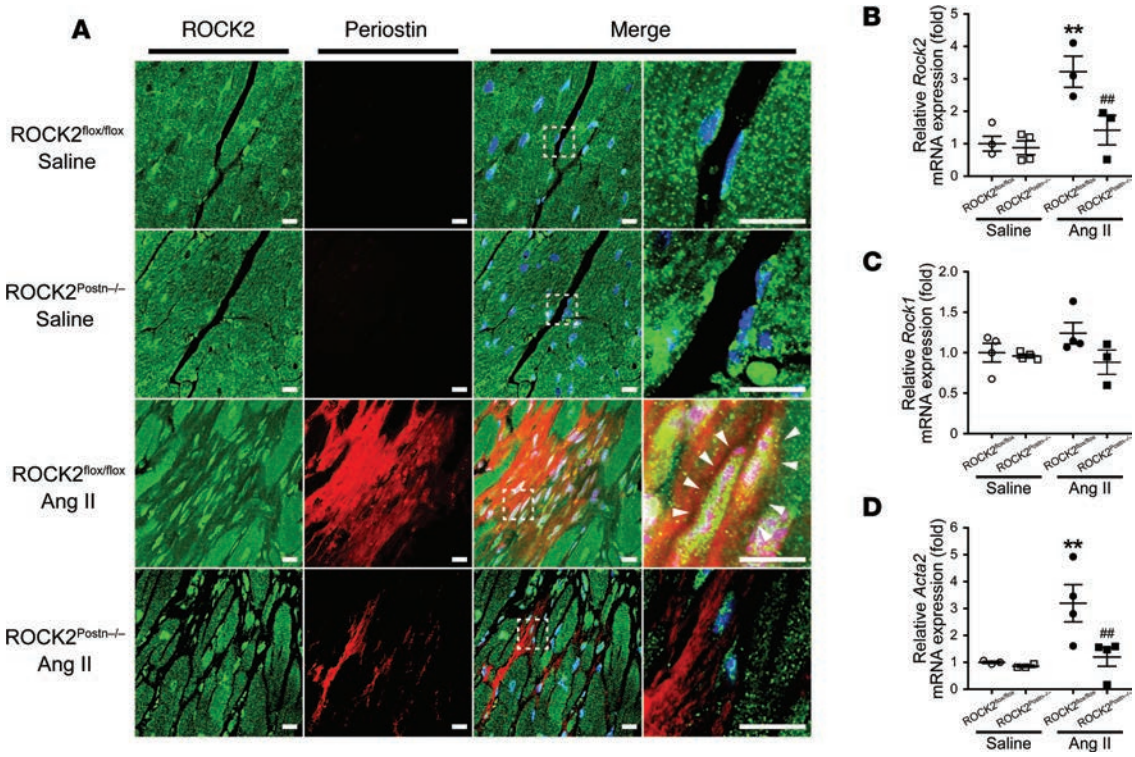

Figure 1. Deletion of ROCK2 in angiotensin II–induced (Ang II–induced) activated cardiac fibroblasts from fibroblast-specific ROCK2-deficient (ROCK2$^{Postn-/-}$) mice. (**A**) Representative fluorescent sections from hearts double-stained with ROCK2 (green) and periostin (red) in ROCK2$^{Postn-/-}$ and littermate control (ROCK2$^{flox/flox}$) mice at 4 wk after saline or Ang II infusion. Nuclei are stained with DAPI (blue). The nuclei of cardiac fibroblasts are elongated in the direction of cardiomyocytes, and their cytoplasms are substantially reduced in volume. Activated cardiac fibroblasts (arrowheads) are identified as periostin-expressing spindle-shaped cells in ROCK2$^{flox/flox}$ mice treated with Ang II (n = 4–5 each). Scale bars: 10 μm. (**B–D**) Quantitative PCR analysis of Rock2, Rock1, and Acta2 (encoding α-smooth muscle actin) mRNA expression in cardiac fibroblasts isolated from ROCK2$^{Postn-/-}$ and ROCK2$^{flox/flox}$ mice treated with saline or Ang II (n = 4–5 each). $^{**}P < 0.01$ vs. saline-treated ROCK2$^{flox/flox}$ mice. $^{\#\#}P < 0.01$ vs. Ang II-treated ROCK2$^{flox/flox}$ mice. Data are expressed as mean ± SEM. P values were calculated using one-way ANOVA with Tukey's HSD test.

Results

Generation and characterization of fibroblast-specific ROCK2-deficient mice. The embryonic lethality associated with global ROCK2$^{-/-}$ mice precludes their use for studying adult models of cardiovascular disease (19). Furthermore, since fibroblasts are heterogeneous cell populations, the characteristics and definition of fibroblast are complex (20), leading to difficulty in interpreting the results of previous studies that investigated the role of fibroblasts in cardiac remodeling. To circumvent this problem, we generated a mouse model in which ROCK2 was conditionally deleted in activated fibroblasts (ROCK2$^{Postn-/-}$), using the promoter of a matricellular protein, periostin, as a Cre-recombinase driver. Periostin is not expressed under basal conditions, but it is markedly upregulated in activated fibroblasts following stress or injury, such as pressure overload or ischemia-reperfusion injury (21–23). Indeed, periostin expression was only observed in heart tissues from mice treated with Ang II (Figure 1A). Following treatment with Ang II, ROCK2 expression was increased in thin, elongated, spindle-shaped activated fibroblasts of littermate controls (ROCK2$^{flox/flox}$) but was absent in ROCK2$^{Postn-/-}$ mice (Figure 1B). ROCK1 expression in activated fibroblasts, however, was comparable among all groups (Figure 1C). The α-smooth muscle actin (α-SMA or *Acta2*) is known to be expressed in myofibroblasts, an activated form of fibroblasts (20). Interestingly, the increase in α-SMA expression following Ang II infusion was also suppressed in fibroblasts from ROCK2$^{Postn-/-}$ mice (Figure 1D). These findings suggest that ROCK2 may be an important mediator of fibroblast to myofibroblast transition.

Fibroblast ROCK2 mediates Ang II–induced cardiac remodeling and diastolic dysfunction. ROCK2$^{Postn-/-}$ mice developed normally over time, were fertile, and were not phenotypically different from littermate controls (ROCK2$^{flox/flox}$ mice) (Supplemental Figure 1A; supplemental material available online with this article; https://doi.org/10.1172/jci.insight.93187DS1). Treatment with Ang II infusion (1,000 ng/kg/min for 4 weeks) decreased body weight to the same extent in both genotypes (Supplemental Figure 1B). In addition, hemodynamic parameters, such as systolic and diastolic blood pressures and heart

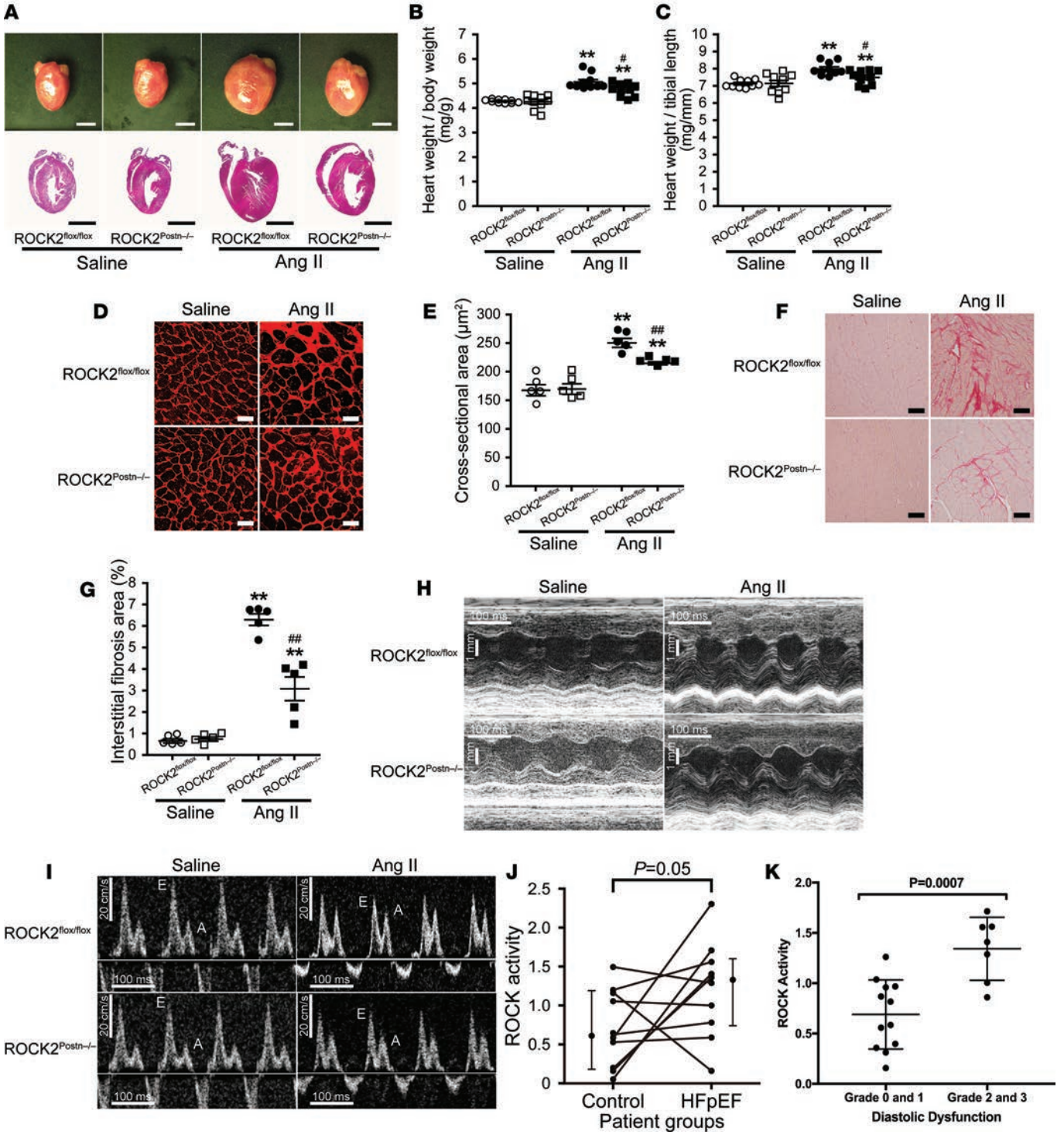

Figure 2. Deletion of ROCK2 in cardiac fibroblasts attenuates angiotensin II–induced (Ang II–induced) cardiac hypertrophy, fibrosis, and diastolic dysfunction. (**A**) Representative photomicrographs and H&E-stained sagittal sections of hearts from fibroblast-specific ROCK2-deficient ($ROCK2^{Postn-/-}$) and littermate control ($ROCK2^{flox/flox}$) mice at 4 wk after saline or Ang II infusion. Scale bars: 3 mm. (**B** and **C**) Quantitative analysis of the ratios of heart weight to body weight and to tibial length from $ROCK2^{Postn-/-}$ and $ROCK2^{flox/flox}$ mice treated with saline or Ang II (n = 10 each). (**D** and **E**) Representative sections from hearts immunostained with wheat germ agglutinin and quantification of cardiomyocyte cross-sectional area in $ROCK2^{Postn-/-}$ and $ROCK2^{flox/flox}$ mice treated with saline or Ang II (n = 5 each). Scale bars: 25 μm. (**F** and **G**) Representative sections from hearts stained with Picrosirius red and quantification of interstitial fibrosis area in $ROCK2^{Postn-/-}$ and $ROCK2^{flox/flox}$ mice treated with saline or Ang II (n = 5 each). Scale bars: 50 μm. (**H**) Representative echocardiographic M-mode images of left ventricles from $ROCK2^{Postn-/-}$ and $ROCK2^{flox/flox}$ mice treated with saline or Ang II (n = 10 each). (**I**) Representative echocardiographic images of mitral inflow pattern to evaluate diastolic dysfunction measured by transmitral Doppler velocity ratio of early-to-atrial wave (E/A ratio) (n = 10 each). $^{**}P < 0.01$ vs. saline-treated each genotype. $^{\#}P < 0.05$, $^{\#\#}P < 0.01$ vs. Ang II–treated $ROCK2^{flox/flox}$ mice. Data are expressed as mean ± SEM. P values were calculated using one-way ANOVA with Tukey's HSD test.

(**J**) Comparison of ROCK activity (phosphorylated myosin-binding subunits [p-MBS]/total MBS [t-MBS]) in HFpEF patients (n = 10) with age- and sex-matched controls (n = 10). Data are expressed as mean ± SEM. P value was calculated using paired t test. (**K**) Relationship between diastolic dysfunction grades and leukocyte ROCK activity (p-MBS/t-MBS) in 19 patients with normal or mild (grades 0 and 1) and moderate to severe (grades 2 and 3) diastolic dysfunction. Mean ROCK activity is higher in patients with moderate to severe compared with normal to mild diastolic dysfunction (1.34 ± 0.31 vs. 0.69 ± 0.34). Data are expressed as mean ± SD. P value was calculated using paired t test.

rate, were comparable between the genotypes at baseline and after saline and were similar after Ang II infusion. (Supplemental Figure 1, E–G). These findings suggest that ROCK2 deficiency in activated fibroblasts from extracardiac sources, including blood vessels and kidneys, does not affect systemic blood pressure. Although Ang II infusion produced a similar increase in blood pressure, the increase in heart weight observed in ROCK2$^{flox/flox}$ mice was suppressed in ROCK2$^{Postn-/-}$ mice (Figure 2, A–C). Consistent with this finding, histological analysis showed that the extent of cellular size and fibrosis — as evaluated by cardiomyocyte cross-sectional area and interstitial collagen deposition area, respectively — were decreased in ROCK2$^{Postn-/-}$ mice compared with ROCK2$^{flox/flox}$ mice (Figure 2, D–G). Indeed, echocardiographic examinations showed that, despite no differences in LV dimensions (LV internal dimension at end-diastole [LVDd] and LV internal dimension at end-systole [LVDs]) and systolic function (fractional shortening [FS] and ejection fraction [EF]) among all groups, Ang II–induced cardiac hypertrophy, as determined by increased LV wall thickness (interventricular septal thickness [IVS] and posterior wall [PW]) and LV mass, was reduced in ROCK2$^{Postn-/-}$ mice compared with littermate controls (Figure 2H and Table 1). Furthermore, diastolic dysfunction observed in ROCK2$^{flox/flox}$ mice after treatment with Ang II, as determined by reduced early-to-atrial wave ratio (E/A ratio) and prolonged isovolumetric relaxation time [IVRT] and %IVRT, was also improved in ROCK2$^{Postn-/-}$ mice (Figure 2I and Table 1). These findings indicate that fibroblast ROCK2 plays a critical role in mediating cardiac hypertrophy and fibrosis — features that are characteristic of LV diastolic dysfunction.

Table 1. Echocardiographic parameters in littermate control (ROCK2$^{flox/flox}$) and fibroblast-specific ROCK2-deficient (ROCK2$^{Postn-/-}$) mice at 4 weeks after treatment

Saline		Ang II	
Parameter	ROCK2$^{flox/flox}$ (n = 10)	ROCK2$^{Postn-/-}$ (n = 10)	ROCK2$^{flox/flox}$ (n = 10)	ROCK2$^{Postn-/-}$ (n = 10)
HR (bpm)	530 ± 32	497 ± 12	544 ± 8	533 ± 13
LVDd (mm)	3.16 ± 0.05	3.13 ± 0.04	3.06 ± 0.04	3.05 ± 0.07
LVDs (mm)	1.85 ± 0.05	1.83 ± 0.04	1.77 ± 0.02	1.76 ± 0.08
IVS (mm)	0.78 ± 0.02	0.78 ± 0.02	1.08 ± 0.01^{B}	1.00 ± 0.01^{D,F}
PW (mm)	0.78 ± 0.02	0.79 ± 0.03	1.11 ± 0.02^{B}	1.01 ± 0.02^{D,E}
FS (%)	40.5 ± 1.4	42.2 ± 1.8	40.1 ± 0.7	40.0 ± 0.6
EF (%)	72.5 ± 1.7	74.3 ± 2.1	72.2 ± 0.8	71.9 ± 0.7
LV mass (mg)	77.7 ± 2.1	77.4 ± 3.0	119.2 ± 3.1^{B}	105.7 ± 3.5^{D,E}
E/A ratio	1.81 ± 0.05	1.85 ± 0.04	1.46 ± 0.03^{B}	1.63 ± 0.01^{D,E}
DT (ms)	18.8 ± 0.5	18.9 ± 0.5	22.1 ± 0.7^{A}	21.2 ± 0.5^{C}
IVRT (ms)	9.5 ± 0.3	9.0 ± 0.3	15.2 ± 0.3^{B}	13.8 ± 0.3^{D,E}
%IVRT	8.8 ± 0.3	8.4 ± 0.3	12.5 ± 0.3^{B}	11.0 ± 0.3^{D,E}

Ang II, angiotensin II; ROCK2$^{flox/flox}$, littermate control mice; ROCK2$^{Postn-/-}$, fibroblast-specific ROCK2-deficient mice; HR, heart rate; LVDd, left ventricular (LV) end–diastolic dimension; LVDs, LV end–systolic dimension; IVS, intraventricular septum; PW, posterior wall; FS, fractional shortening; EF, ejection fraction; E/A ratio, transmitral early-to-atrial wave ratio; DT, deceleration time; IVRT, isovolumetric relaxation time; %IVRT, corrected IVRT. Comparisons were performed using one-way ANOVA. $^{A}P < 0.05$, $^{B}P < 0.01$ vs. saline-treated ROCK2$^{flox/flox}$; $^{C}P < 0.05$, $^{D}P < 0.01$ vs. saline-treated ROCK2$^{Postn-/-}$; $^{E}P < 0.05$, $^{F}P < 0.01$ vs. Ang II–treated ROCK2$^{flox/flox}$. Results are expressed as mean ± SEM. P values were calculated using one-way ANOVA with Tukey's HSD test.

Relationship between ROCK activity and LV diastolic dysfunction in humans. Because leukocyte ROCK activity increases with age, we identified 10 with age- and sex- matched controls, with a mean age of 66 ± 7 and 70% female. Compared with controls, patients with LV diastolic dysfunction had higher mean serum creatinine (2.4 ± 2.0 versus 0.9 ± 0.2 mg/dl, $P < 0.05$) and higher rates of hypertension (100% versus 50%, $P < 0.05$) and diabetes (70% versus 10%, $P < 0.05$). In age-matched pairs, leukocyte ROCK activity was higher in patients with diastolic dysfunction than in control subjects (median 1.33 [interquartile range 0.74, 1.6] vs. 0.61 [0.18, 1.19], $P = 0.05$) (Figure 2J). In 19 patients with LV diastolic dysfunction who were analyzed by echocardiography, 7 had diastolic dysfunction grades of 0 and 1 (normal to mild), and 12 had diastolic dysfunction grades of 2 and 3 (moderate to severe). There was higher ROCK activity in patients with moderate to severe diastolic dysfunction compared with those with normal or mild diastolic dysfunction (mean 1.34 ± 0.31 vs. 0.69 ± 0.34, $P = 0.0007$) (Figure 2K and Supplemental Figure 2D).

Increased fibroblast ROCK activity augments Ang II–induced cardiac remodeling and diastolic dysfunction. To test whether increased fibroblast ROCK2 activity is sufficient to mediate cardiac hypertrophy and diastolic dysfunction, we developed a fibroblast-specific constitutively active ROCK knock-in (caROCK$^{Postn-/-}$) mouse, which exhibited normal growth and no physiological abnormalities compared with littermate controls (caROCK$^{flox/flox}$ mice) (Supplemental Figure 1C). Similar to the results of ROCK2$^{Postn-/-}$ mice, Ang II treatment reduced body weight gain and elevated systolic and diastolic pressure to the same

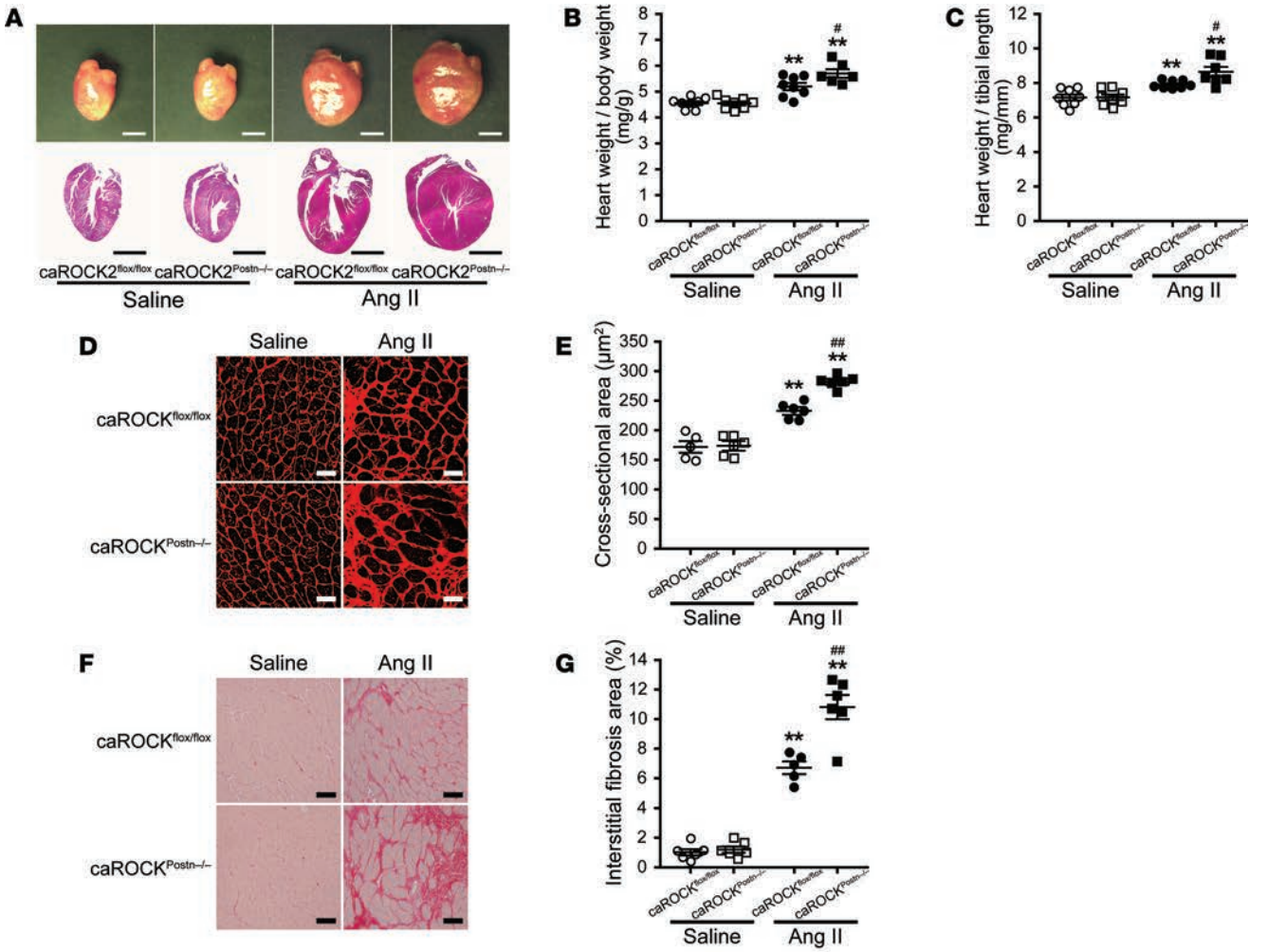

Figure 3. ROCK activation in cardiac fibroblasts develops angiotensin II–induced (Ang II–induced) cardiac hypertrophy, fibrosis, and diastolic dysfunction. (**A**) Representative photomicrographs and H&E-stained sagittal sections of hearts from fibroblast-specific constitutively active ROCK knock-in (caROCK$^{Postn-/-}$) and littermate control (caROCK$^{flox/flox}$) mice at 4 wk after saline or Ang II infusion. Scale bars: 3 mm. (**B** and **C**) Quantitative analysis of the ratios of heart weight to body weight and to tibial length from caROCK$^{Postn-/-}$ and caROCK$^{flox/flox}$ mice treated with saline or Ang II (n = 6–8 each). (**D** and **E**) Representative sections from hearts immunostained with wheat germ agglutinin and quantification of cardiomyocyte cross-sectional area in caROCK$^{Postn-/-}$ and caROCK$^{flox/flox}$ mice treated with saline or Ang II (n = 5–6 each). Scale bars: 25 μm. (**F** and **G**) Representative sections from hearts stained with Picrosirius red and quantification of interstitial fibrosis area in caROCK$^{Postn-/-}$ and caROCK$^{flox/flox}$ mice treated with saline or Ang II (n = 5–6 each). Scale bars: 50 μm. (**H**) Representative echocardiographic M-mode images of left ventricles from caROCK$^{Postn-/-}$ and caROCK$^{flox/flox}$ mice treated with saline or Ang II (n = 8–10 each). (**I**) Representative echocardiographic images of mitral inflow pattern to evaluate diastolic dysfunction measured by transmitral Doppler velocity ratio of early-to-atrial wave (E/A ratio) (n = 8–10 each). $^{**}P < 0.01$ vs. saline-treated each genotype. $^{\#}P < 0.05$, $^{\#\#}P < 0.01$ vs. Ang II–treated caROCK$^{flox/flox}$ mice. Data are expressed as mean ± SEM. P values were calculated using one-way ANOVA with Tukey's HSD test.

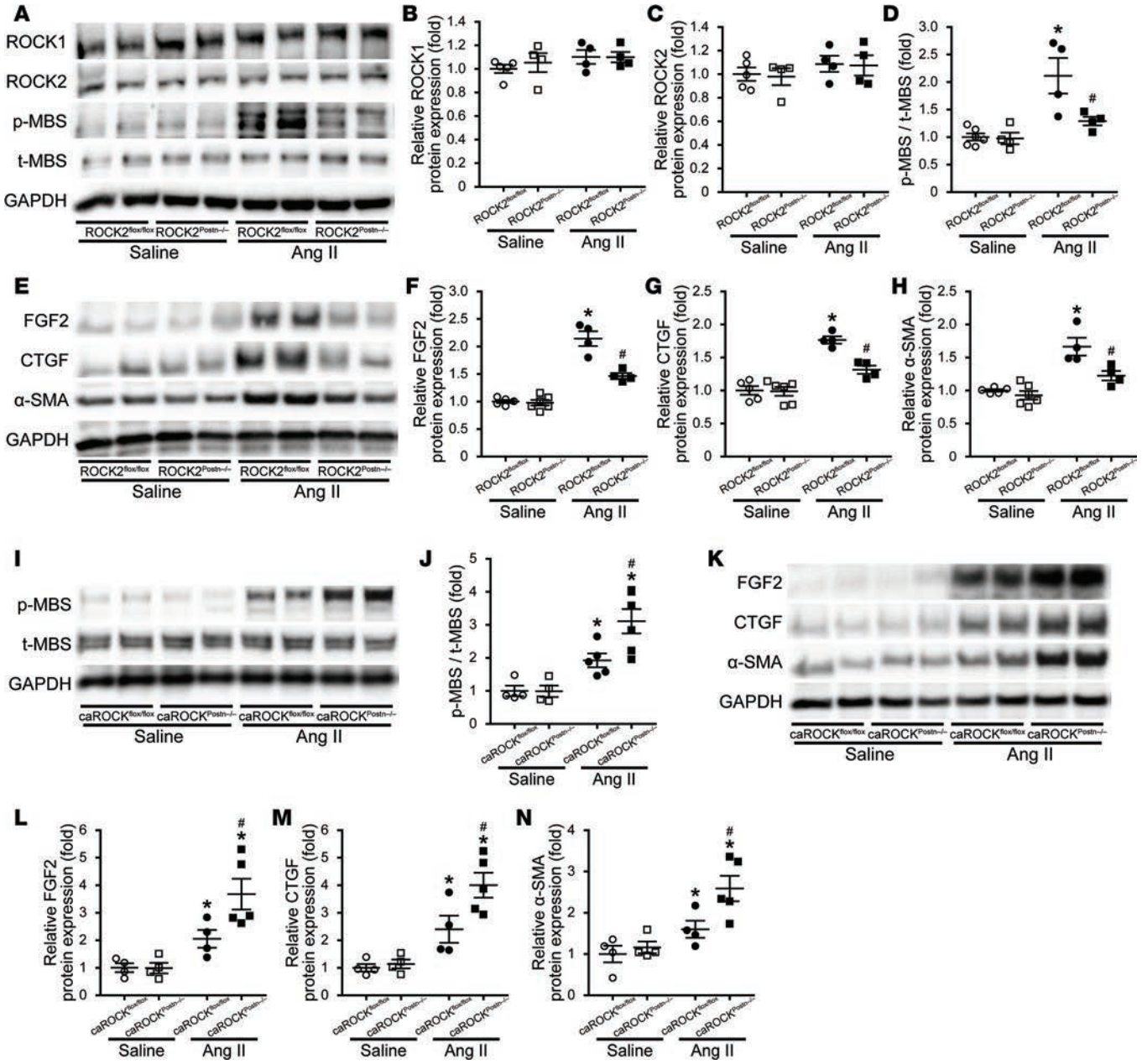

Figure 4. ROCK2 in cardiac fibroblasts is involved in angiotensin II–induced (Ang II–induced) cardiac remodeling through regulation of FGF2, CTGF, and α-SMA expression. Fibroblast-specific ROCK2-deficient ($ROCK2^{Postn-/-}$) and littermate control ($ROCK2^{flox/flox}$) mice (**A–H**), and fibroblast-specific constitutively active ROCK knock-in ($caROCK^{Postn-/-}$) and littermate control ($caROCK^{flox/flox}$) mice (**I–N**) were treated with saline or Ang II for 4 wk. (**A** and **I**) Representative immunoblots of ROCK1, ROCK2, and ROCK activity, as assessed by the ratio of phosphorylated form of the myosin-binding subunit (MBS) to total MBS (p-MBS/t-MBS), in heart tissues from each experimental genotype. (**B** and **C**) Quantification of ROCK1 and ROCK2 protein expression, and (**D** and **J**) ROCK activity levels by densitometry (n = 4–6 each). (**E** and **K**) Representative immunoblots of FGF2, CTGF, and α-SMA in heart tissues from each experimental genotype. (**F–H** and **L–N**) Quantification of FGF2, CTGF, and α-SMA protein expression by densitometry (n = 4–6 each). $^{*}P < 0.05$ vs. saline-treated each genotype. $^{\#}P < 0.05$ vs. Ang II–treated respective controls. Data are expressed as mean ± SEM. P values were calculated using one-way ANOVA with Tukey's HSD test.

extent in both genotypes, without affecting heart rate (Supplemental Figure 1, D and H–J). Expression of the knock-in allele and higher ROCK activity in activated fibroblasts from $caROCK^{Postn-/-}$ mice was confirmed after treatment with Ang II (Supplemental Figure 2, A–C). Furthermore, increase in heart weight, cardiomyocyte hypertrophy, and interstitial fibrosis were greater in $caROCK^{Postn-/-}$ compared with $caROCK^{flox/flox}$ mice following Ang II infusion (Figure 3, A–G). These findings are in agreement with echocardiography, which showed a greater degree of cardiac hypertrophy and diastolic dysfunction in $caROCK^{Postn-/-}$ mice compared with littermate controls ($caROCK^{flox/flox}$ mice) following Ang II infusion (Figure 3, H and I, and Table 2).

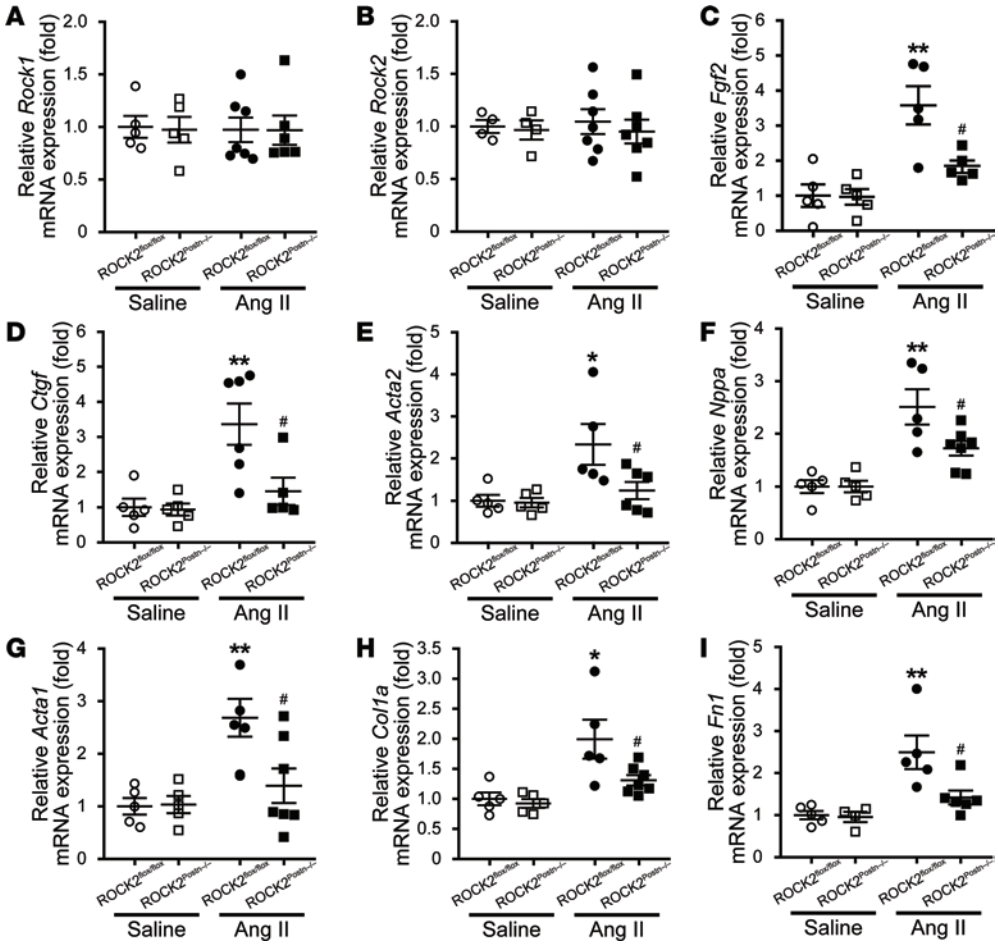

Figure 5. Decreased gene expression related to cardiac hypertrophy, fibrosis, and fibroblast to myofibroblast differentiation in hearts from fibroblast-specific ROCK2-deficient (ROCK2$^{Postn-/-}$) mice treated with angiotensin II (Ang II). (**A** and **B**) Quantitative PCR analysis mRNA levels of Rock1 and Rock2; (**C**) a prohypertrophic mediator of Fgf2 (encoding fibroblast growth factor 2); (**D**) a profibrotic mediator of Ctgf (connective tissue growth factor); (**E**) a fibroblast-myoblast differentiation marker, Acta2 (α-smooth muscle actin); (**F** and **G**) hypertrophic markers of Nppa (atrial natriuretic factor) and Acta1 (skeletal muscle α-actin); and (**H** and **I**) fibrotic markers of Col1a (collagen type I) and Fn1 (fibronectin 1) in heart tissues from ROCK2$^{Postn-/-}$ and littermate control (ROCK2$^{flox/flox}$) mice at 4 wk after saline or Ang II infusion (n = 4–7 each). $^{*}P <$ 0.05, $^{**}P < 0.01$ vs. saline-treated ROCK2$^{flox/flox}$ mice. $^{\#}P < 0.05$ vs. Ang II–treated ROCK2$^{flox/flox}$ mice. Data are expressed as mean ± SEM. P values were calculated using one-way ANOVA with Tukey's HSD test.

These findings indicate that increased fibroblast ROCK activity is sufficient to induce cardiac hypertrophy, fibrosis, and diastolic dysfunction following Ang II infusion.

ROCK2 mediates hypertrophic and fibrotic signaling pathways in cardiac remodeling. To determine the potential downstream mechanisms involved, we next examined whether protein and gene expression that are related to cardiac remodeling were altered in the hearts from ROCK2$^{Postn-/-}$ after treatment with Ang II. Among all groups, there were no differences in the expression of both ROCK1 and ROCK2 in heart tissues, the main volume of which are occupied by cardiomyocytes (CMs) (24). However, Ang II–induced ROCK activation was suppressed in ROCK2$^{Postn-/-}$ compared with ROCK2$^{flox/flox}$ mice (Figure 4, A–D, and Figure 5, A and B). Ang II infusion increased expression of key mediators of cardiac hypertrophy, fibrosis, and fibroblast-myofibroblast differentiation, namely fibroblast growth factor–2 (FGF2), connective tissue growth factor (CTGF), and α-SMA, in heart tissues from ROCK2$^{flox/flox}$ mice. These increases were suppressed in ROCK2$^{Postn-/-}$ mice (Figure 4, E–H, and Figure 5, C–E). Similar findings were observed with hypertrophic markers such as atrial natriuretic factor (ANF), skeletal muscle α-actin (α-SK), and β-MHC; fibrotic markers of collagen I and fibronectin 1; and a central mediator in the pathogenesis of cardiac remodeling, transforming growth factor (TGF-β1) (Figure 5, F–I, and Supplemental Figure 3, A–E). We have previously shown that ROCK2 in cardiomyocytes enhances apoptosis and MAPK pathway in the development of Ang II–induced cardiac remodeling, through activation of cleaved caspase–3 and extracellular signal-regulated kinase (ERK), respectively (15). Similarly, Ang II–enhanced apoptosis was reduced in heart tissues of ROCK2$^{Postn-/-}$ mice. (Supplemental Figure 3, A and F). Furthermore, phosphorylation of p38 and ERK, but not stress-activated protein kinase (SAPK), in response to Ang II were reduced in ROCK2$^{Postn-/-}$ mice (Supplemental Figure 3, F–J). In contrast, Ang II–induced increase in FGF2, CTGF, and α-SMA were augmented in heart tissues from caROCK$^{Postn-/-}$ mice compared with littermate controls (Figure 4, I–N). Similar results were also obtained in the cases of hypertrophic markers of ANF and β-MHC, a fibrotic marker of collagen I,

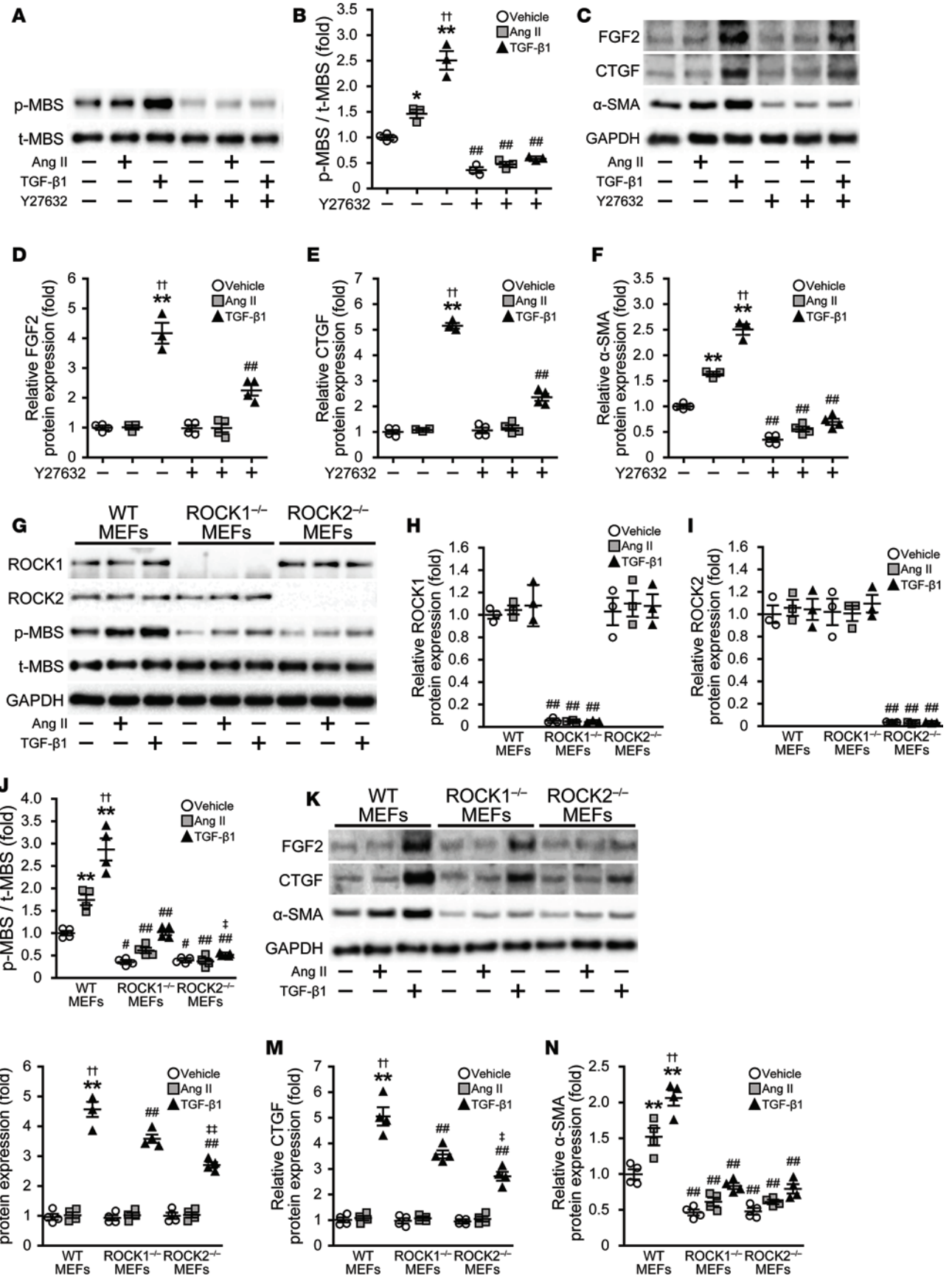
A
p-MBS
t-MBS
Ang II
TGF-β1
Y27632
B
p-MBS / t-MBS (fold)
Vehicle
Ang II
TGF-β1
C
FGF2
CTGF
α-SMA
GAPDH
D
Relative FGF2 protein expression (fold)
E
Relative CTGF protein expression (fold)
F
Relative α-SMA protein expression (fold)
G
WT MEFs
ROCK1−/− MEFs
ROCK2−/− MEFs
ROCK1
ROCK2
H
Relative ROCK1 protein expression (fold)
I
Relative ROCK2 protein expression (fold)
J
K
L
M
N

Figure 6. Effects of ROCK deletion on the activated mediators related to cardiac remodeling in response to angiotensin II (Ang II) or TGF-β1 in mouse embryonic fibroblasts (MEFs). (**A** and **B**) Representative immunoblots and densitometric quantification of ROCK activity, as assessed by the ratio of phosphorylated form of the myosin-binding subunit (MBS) to total MBS (p-MBS/t-MBS), stimulated by 1 μM Ang II or 10 ng/ml TGF-β1 for 24 hours, with or without 10 μM Y27632, a specific ROCK inhibitor, in MEFs isolated from WT mice (n = 3–4 each). (**C–F**) Representative immunoblots and densitometric quantification of FGF2, CTGF, and α-SMA protein expression, stimulated by Ang II or TGF-β1, with or without Y27632, in WT MEFs (n = 3–4 each). $^{*}P < 0.05$, $^{**}P < 0.01$ vs. vehicle-stimulated WT MEFs. $^{\#\#}P < 0.01$ vs. the same stimulated WT MEFs without Y27632. $^{\dagger\dagger}P < 0.01$ vs. Ang II–stimulated WT MEFs without Y27632. (**G–J**) Representative immunoblots and densitometric quantification of ROCK1 and ROCK2 protein expression and ROCK activity, as assessed by the ratio of phosphorylated form of the myosin-binding subunit (MBS) to total MBS (p-MBS/t-MBS), stimulated by Ang II or TGF-β1, in MEFs isolated from WT, global Rock1-KO (ROCK1$^{-/-}$), and global Rock2-KO (ROCK2$^{-/-}$) mice (n = 3–4 each). (**K–N**) Representative immunoblots and densitometric quantification of FGF2, CTGF, and α-SMA protein expression, stimulated by Ang II or TGF-β1, in WT, global ROCK1$^{-/-}$, and global ROCK2$^{-/-}$ MEFs (n = 3–4 each). $^{**}P < 0.01$ vs. vehicle-stimulated WT MEFs. $^{\#}P < 0.05$, $^{\#\#}P < 0.01$ vs. the same stimulated WT MEFs. $^{\dagger\dagger}P < 0.01$ vs. Ang II–stimulated WT MEFs. $^{\ddagger}P < 0.05$, $^{\ddagger\ddagger}P < 0.01$ vs. TGF-β1-stimulated global ROCK1$^{-/-}$ MEFs. Data are expressed as mean ± SEM. P values were calculated using one-way ANOVA with Tukey's HSD test.

an apoptosis marker of cleaved caspase-3, and MAPK pathways of p38 and ERK (Supplemental Figure 4, A–H). Taken together, these findings indicate that fibroblast ROCK2 is an important regulator of hypertrophic and fibrotic signaling pathways in the heart.

Role of ROCKs in the regulation of CTGF, FGF2, and α-SMA gene expression in fibroblasts in vitro. To further elucidate the mechanisms underlying ROCK2-mediated cardiac hypertrophy, fibrosis, and myofibroblast differentiation by Ang II, we focused on FGF2, CTGF, and α-SMA, respectively, among the CF-related genes examined in mouse heart tissues. We generated mouse embryonic fibroblasts (MEFs) from WT mice. The increase in ROCK activity was observed in WT MEFs treated with Ang II and more in those with TGF-β1, and both were completely blocked by the ROCK inhibitor Y27632 (Figure 6, A and B). However, despite the increase in α-SMA expression in response to Ang II and TGF-β1, the expression of FGF2 and CTGF were increased in WT MEFs treated with TGF-β1 alone. All of the increases were also suppressed by Y27632 (Figure 6, C–F, and Figure 7, A–C). Importantly, these results are consistent with previous studies suggesting that TGF-β1 acts downstream of Ang II in CFs and directly stimulates CFs (25). Therefore, we used TGF-β1 in addition to Ang II in our in vitro study.

In addition, using MEFs derived from mice with global homozygous deletion of ROCK1 (ROCK1$^{-/-}$) or ROCK2 (ROCK2$^{-/-}$) (Figure 6, G–I), we found a decrease in TGF-β1–induced ROCK activity and a reduction FGF2 and CTGF expression in ROCK2$^{-/-}$ MEFs compared with ROCK1$^{-/-}$ or WT MEFs, whereas α-SMA expression was reduced to a similar extent in ROCK1$^{-/-}$ and ROCK2$^{-/-}$MEFs compared with WT MEFs (Figure 6, G, J–N, and Figure 7, D–F).

To confirm the role of ROCKs in CFs, we also examined rat neonatal cardiac fibroblasts (RNCFs) treated with Y27632 and those transfected with ROCK1 or ROCK2 siRNA, showing efficient knockdown of ROCK1 or ROCK2 (Supplemental Figure 5, A–C, and Figure 8, G–I). Similar to the results observed in MEFs, TGF-β1–induced increase in ROCK activity and expression of FGF2 and CTGF were suppressed in RNCFs treated with Y27632 and those transfected with ROCK2 siRNA compared with ROCK1 siRNA (Figure 8, A–E, G, and J–M). Transfection with either ROCK1 or ROCK2 siRNA also markedly reduced TGF-β1–induced increase in α-SMA expression in RNCFs, similar to those treated with Y27632 (Figure 8, C, F, K, and N). These findings suggest that fibroblast ROCK2, through its ability to upregulate CTGF, FGF2, and α-SMA in response to TGF-β1, is an important mediator of cardiac remodeling.

Table 2. Echocardiographic parameters in littermate control (caROCK$^{flox/flox}$) and fibroblast-specific constitutively active ROCK–knock-in (caROCK$^{Postn-/-}$) mice at 4 weeks after treatment

	Saline		Ang II	
Parameter	**caROCK$^{flox/flox}$ (n = 10)**	**caROCK$^{Postn-/-}$ (n = 10)**	**caROCK$^{flox/flox}$ (n = 8)**	**caROCK$^{Postn-/-}$ (n = 8)**
HR (bpm)	481 ± 14	482 ± 17	523 ± 15	525 ± 20
LVDd (mm)	3.09 ± 0.05	3.12 ± 0.03	3.02 ± 0.05	2.89 ± 0.03^{B,D}
LVDs (mm)	1.84 ± 0.03	1.82 ± 0.02	1.76 ± 0.01	1.64 ± 0.02^{B,D}
IVS (mm)	0.77 ± 0.02	0.78 ± 0.01	1.04 ± 0.01^{A}	1.19 ± 0.02^{B,D}
PW (mm)	0.78 ± 0.01	0.77 ± 0.01	1.06 ± 0.03^{A}	1.20 ± 0.02^{B,D}
FS (%)	40.5 ± 0.7	41.6 ± 0.6	41.8 ± 0.6	43.2 ± 0.7
EF (%)	72.7 ± 0.8	74.0 ± 0.7	74.3 ± 0.6	76.0 ± 0.7
LV mass (mg)	74.7 ± 1.8	75.7 ± 2.0	113.0 ± 2.1^{A}	129.7 ± 3.2^{B,D}
E/A ratio	1.85 ± 0.05	1.89 ± 0.03	1.51 ± 0.03^{A}	1.23 ± 0.04^{B,D}
DT (ms)	18.9 ± 0.6	18.1 ± 0.5	23.4 ± 0.2^{A}	25.9 ± 0.2^{B,C}
IVRT (ms)	9.0 ± 0.4	8.6 ± 0.4	14.7 ± 0.2^{A}	16.2 ± 0.3^{B,C}
%IVRT	8.5 ± 0.3	8.3 ± 0.3	12.8 ± 0.3^{A}	14.7 ± 0.7^{B,C}

Ang II, angiotensin II; caROCK$^{flox/flox}$, littermate control mice; caROCK$^{Postn-/-}$, fibroblast-specific constitutively active knock-in ROCK mice; HR, heart rate; LVDd, left ventricular (LV) end–diastolic dimension; LVDs, LV end–systolic dimension; IVS, intraventricular septum; PW, posterior wall; FS, fractional shortening; EF, ejection fraction; E/A ratio, transmitral early-to-atrial wave ratio; DT, deceleration time; IVRT, isovolumetric relaxation time; %IVRT, corrected IVRT. Comparisons were performed using one-way ANOVA. $^{A}P < 0.01$ vs. saline-treated caROCK$^{flox/flox}$; $^{B}P < 0.01$ vs. saline-treated caROCK$^{Postn-/-}$; $^{C}P < 0.05$, $^{D}P < 0.01$ vs. Ang II-treated caROCK$^{flox/flox}$. Results are expressed as mean ± SEM. P values were calculated using one-way ANOVA with Tukey's HSD test.

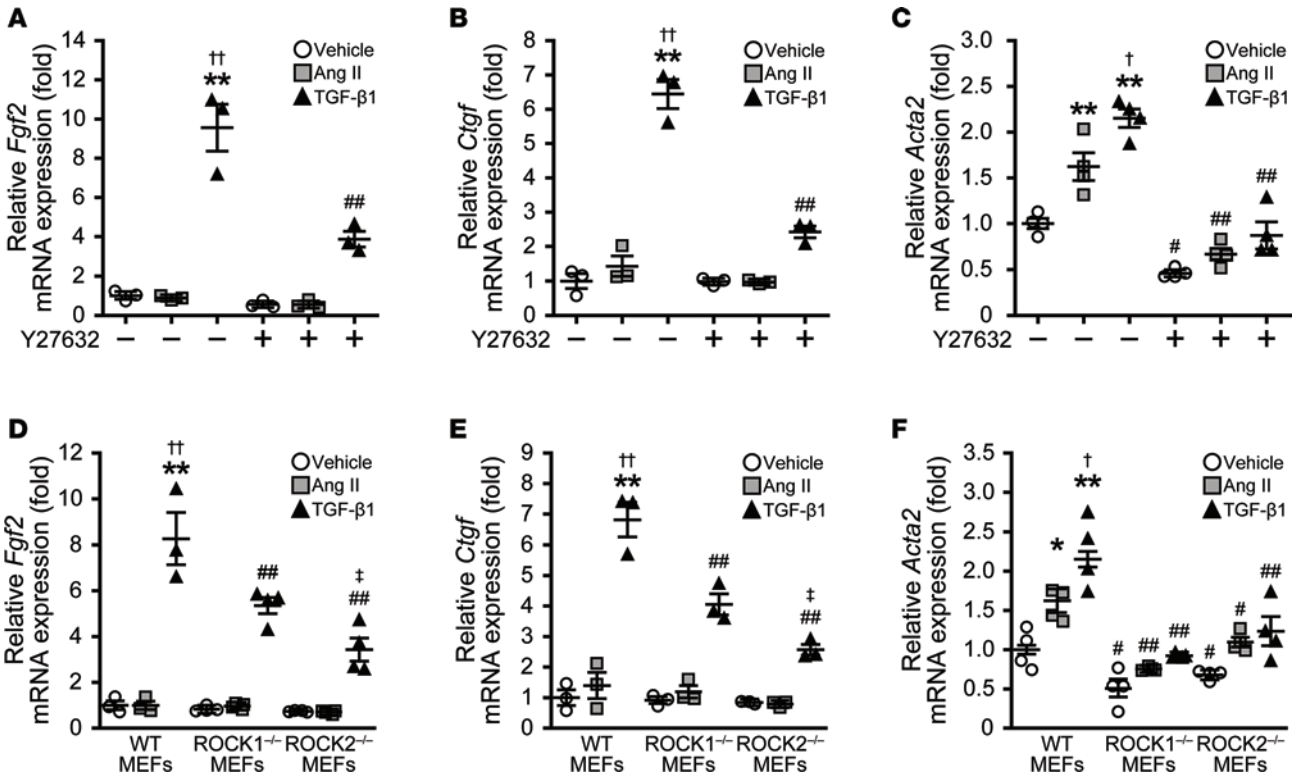

Figure 7. Effects of ROCK deletion on mRNA expression of FGF2, CTGF, and α-SMA in response to angiotensin II (Ang II) or transforming growth factor-β1 (TGF-β1) in mouse embryonic fibroblasts (MEFs). (**A–C**) Quantitative PCR analysis of Fgf2 (encoding fibroblast growth factor 2), Ctgf (connective tissue growth factor), and Acta2 (α-smooth muscle actin) mRNA expression stimulated by 1 μM Ang II or 10 ng/ml TGF-β1 for 24 hours, with or without 10 μM Y27632, a specific ROCK inhibitor, in MEFs isolated from WT (n = 3–4 each). $^{**}P < 0.01$ vs. vehicle-stimulated WT MEFs. $^{\#}P < 0.05$, $^{\#\#}P < 0.01$ vs. the same stimulated WT MEFs without Y27632. $^{\dagger}P < 0.05$, $^{\dagger\dagger}P < 0.01$ vs. Ang II–stimulated WT MEFs without Y27632. (**D–F**) Quantitative PCR analysis of Fgf2, Ctgf, and Acta2 mRNA expression stimulated by 1 μM Ang II or 10 ng/ml TGF-β1 for 24 hours in MEFs isolated from WT, global Rock1-KO (ROCK1$^{-/-}$), and global Rock2-KO (ROCK2$^{-/-}$) mice (n = 3–4 each). $^{*}P < 0.01$, $^{**}P < 0.01$ vs. vehicle-stimulated WT MEFs. $^{\#}P < 0.05$, $^{\#\#}P < 0.01$ vs. the same stimulated WT MEFs. $^{\dagger}P < 0.05$, $^{\dagger\dagger}P < 0.01$ vs. Ang II–stimulated WT MEFs. $^{\ddagger}P < 0.05$ vs. TGF-β1–stimulated global ROCK1$^{-/-}$ MEFs. Data are expressed as mean ± SEM. P values were calculated using one-way ANOVA with Tukey's HSD test.

FGF2 as a ROCK2-dependent paracrine mediator of cardiac hypertrophy. To determine whether FGF2 could be the hypertrophic mediator, we assessed the role of fibroblast ROCK2 in the extracellular release of FGF2. TGF-β1 treatment of RNCFs led to increased extracellular FGF2 as well as extracellular CTGF, which were attenuated by Y27632 and transfection with ROCK2 siRNA, but not ROCK1 siRNA (Figure 9, A–D). Indeed, FGF2 induced a dose-dependent increase in cell size in rat H9C2 cardiomyocytes (Figure 9, E and F), along with upregulation of hypertrophic markers of α-SK, β-MHC, and ANF (Figure 9, G–I). Finally, to determine whether FGF2's effect on cardiac hypertrophy is fibroblast ROCK2–dependent, we performed coculture experiments with RNCFs and H9C2 cardiomyocytes. Both cell size and expression of hypertrophic markers of α-SK, β-MHC, and ANF were increased in H9C2 cardiomyocytes after incubation with conditioned medium from RNCFs treated with TGF-β1 for 24 hours and subsequently neutralized with anti–TGF-β1 antibody. Importantly, these increases were absent in H9C2 cardiomyocytes after incubation with conditioned medium from TGF-β1–treated RNCFs with Y27632 (Figure 10, A–E) or those transfected with ROCK2 siRNA, but not ROCK1 siRNA (Figure 10, F–J). Taken together, these findings indicate that FGF2 is a fibroblast ROCK2–dependent paracrine mediator of cardiac hypertrophy.

Discussion

We have shown that fibroblast-specific ROCK2 is a critical mediator of cardiac hypertrophy, fibrosis, and diastolic dysfunction through upregulation of profibrotic (CTGF), prohypertrophic (FGF2), and promyofibroblast differentiation (α-SMA) genes. Using loss-of-function of ROCK2 (ROCK2$^{Postn-/-}$) and gain-of-function of ROCK (caROCK$^{Postn+/-}$) mutant mice, we showed that fibroblast ROCK2 is necessary and sufficient for mediating Ang II–induced cardiac hypertrophy, fibrosis, and remodeling. Thus, fibroblast ROCK2

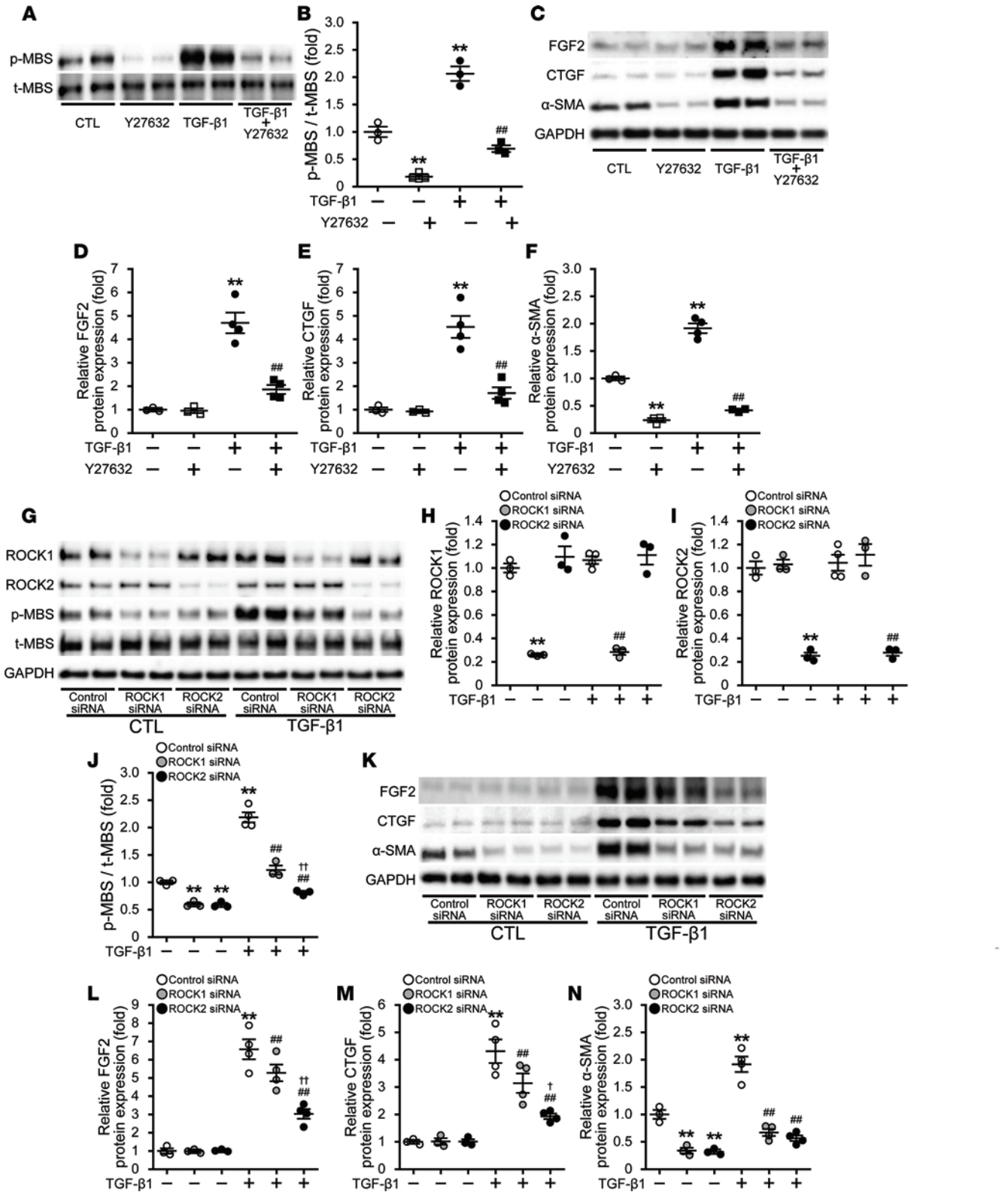

Figure 8. Effects of ROCK knockdown on the activated mediators related to cardiac remodeling in response to TGF-β1 in rat neonatal cardiac fibroblasts (RNCFs). (**A** and **B**) Representative immunoblots and densitometric quantification of ROCK activityas assessed by the ratio of phosphorylated form of the myosin-binding subunit (MBS) to total MBS (p-MBS/t-MBS), stimulated by 10 ng/ml TGF-β1 for 24 hours, with or without 10 μM Y27632, a specific ROCK inhibitor, in RNCFs (n = 3–4 each). (**C–F**) Representative immunoblots and densitometric quantification of FGF2, CTGF, and α-SMA protein expression, stimulated by TGF-β1, with or without Y27632, in RNCFs (n = 3–4 each). $^{**}P < 0.01$ vs. vehicle-stimulated RNCFs. $^{\#\#}P < 0.01$ vs. TGF-β1–stimulated RNCFs without Y27632. (**G–J**) Representative immunoblots and densitometric quantification of ROCK1 and ROCK2 protein expression and ROCK activity, stimulated by TGF-β1, in RNCFs transfected with control, ROCK1, or ROCK2 siRNA (n = 3–4 each). (**K–N**) Representative

immunoblots and densitometric quantification of FGF2, CTGF, and α-SMA protein expression, stimulated by TGF-β1, in RNCFs transfected with control, ROCK1, or ROCK2 siRNA (n = 3–4 each). $^{**}P < 0.01$ vs. vehicle-stimulated RNCFs transfected with control siRNA. $^{\#\#}P < 0.01$ vs. TGF-β1–stimulated RNCFs transfected with control siRNA. $^{\dagger}P < 0.05$, $^{\dagger\dagger}P < 0.01$ vs. TGF-β1–stimulated RNCFs transfected with ROCK1 siRNA. Data are expressed as mean ± SEM. P values were calculated using one-way ANOVA with Tukey's HSD test.

appears to be an important pathogenic mediator of diastolic dysfunction, and elevated leukocyte ROCK activity correlates with the severity of diastolic dysfunction in humans. Indeed, ventricular structure and function in hearts with diastolic dysfunction is marked by myocyte hypertrophy, concentric LV remodeling, and end-diastolic stiffness (26). The underlying mechanism is due, in part, to ROCK2-dependent expression of FGF2 and CTGF in fibroblasts, which acts in a paracrine manner to elicit cardiomyocyte hypertrophy and cardiac fibrosis. These findings are consistent with previous animal studies showing that nonselective ROCK inhibitors can prevent the development of cardiac hypertrophy and fibrosis, and that ROCK2 rather than ROCK1 is the primary mediator of cardiac hypertrophy (10, 15, 27, 28).

One of the main cellular features of diastolic dysfunction is the activation of fibroblasts, which in turn increase type I collagen production and reduce matrix metalloproteinase–1 activity, thereby increasing diastolic stiffness through collagen deposition in the extracellular matrix (29). TGF-β is an important regulator of the extracellular matrix and is one of the most prominent mediators of cardiac hypertrophy, fibrosis, and remodeling (25). Among the three isoforms of TGF-β, TGF-β1 is the predominant isoform in the cardiovascular system and acts as the downstream mediator of Ang II (30, 31). Ang II alone is unable to induce cardiac remodeling in vivo in the absence of TGF-β1 (32). We found that Ang II induces the expression of TGF-β1 in vivo and that TGF-β1 is a potent stimulator of fibroblast activation, and FGF2 and CTGF expression, in MEFs and RNCFs in vitro. A critical profibrotic downstream target gene of TGF-β signaling is CTGF, which is a matricellular protein that acts in concert with TGF-β1 to induce fibrogenesis (33). Importantly, CTGF is predominantly expressed in activated CFs and, along with the myofibroblast differentiation marker α-SMA, is transcriptionally induced by the myocardin-related transcription factor (MRTF)/serum response factor (SRF) in a ROCK-dependent manner (34, 35). Indeed, the upregulation of CTGF, α-SMA, and other fibrotic markers in the heart after Ang II infusion was attenuated in ROCK2$^{Postn-/-}$ mice and augmented in caROCK$^{Postn-/-}$ mice. These findings suggest a critical role of ROCK2 in mediating the MRTF/SRF pathway in myofibroblast differentiation and fibrosis.

An important paracrine growth factor, which could promote cardiac hypertrophy via FGFR1c and subsequent MAPK activation, is FGF2 (36). Previous studies using FGF2-deficient and -overexpressing mutant mice have shown that FGF2 is a critical mediator of cardiac hypertrophy in response to transaortic constriction (TAC) or renal-induced hypertension (37–39). Similar to the expression of CTGF, FGF2 is mainly synthesized by CFs in response to myocardial stress (40, 41). We found that the expression of FGF2 and other hypertrophic markers, as well as the activation of ERK and p38 MAPK, were increased in heart tissues after Ang II infusion. The importance of fibroblast ROCK2 in mediating these processes is underscored by the suppression and enhancement of cardiac hypertrophy in ROCK2$^{Postn-/-}$ and caROCK $^{Postn-/-}$ mice, respectively. These findings are in agreement with previous studies showing that the development of cardiac hypertrophy in response to Ang II or TAC was attenuated in global ROCK2$^{+/-}$ mice, but not in ROCK1$^{+/-}$ or ROCK1$^{-/-}$ mice (13–15), despite 92% homology between ROCK1 and ROCK2 in their N-terminal kinase domains (42). Using coculture assay, we further demonstrate that FGF2 from fibroblasts are able to induce cardiomyocyte hypertrophy in a paracrine- and ROCK2-dependent manner. These findings suggest that the ROCK2/FGF2 pathway in fibroblasts is critically important in mediating the development of cardiac hypertrophy, fibrosis, and diastolic dysfunction.

Although the pathogenic mechanisms leading to the development of LV diastolic dysfunction remain unknown (43), we found that echocardiographic measurements of Ang II–induced diastolic dysfunction were reduced in ROCK2$^{Postn-/-}$ mice and worsened in caROCK $^{Postn-/-}$ mice. Furthermore, leukocyte ROCK activity was elevated in age- and sex-matched patients with diastolic dysfunction compared with controls, and increased leukocyte ROCK activity was associated with greater severity of diastolic dysfunction. These findings, therefore, suggest that selective inhibition of fibroblast ROCK2 could be a novel therapeutic approach for preventing cardiac hypertrophy and fibrosis, and for the development of diastolic dysfunction. However, it remains to be determined whether the current mouse model used for diastolic dysfunction is generalizable to HF with preserved ejection fraction (HFpEF) in humans, where different etiologies may contribute, and whether CFs from patients with HFpEF and diastolic dysfunction have elevated ROCK2 expression and activity.

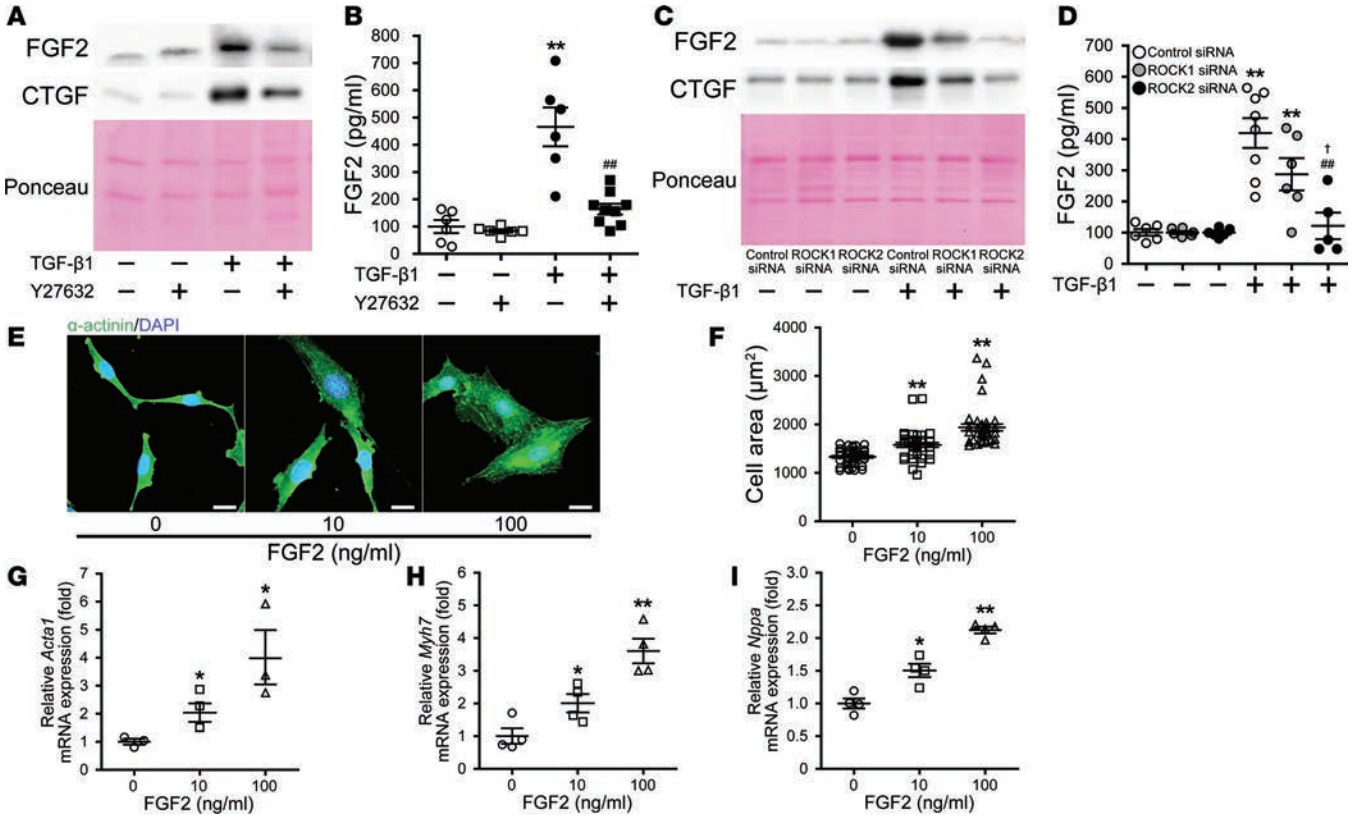

Figure 9. Inhibition of ROCK2 decreases extracellular release of FGF2 from rat neonatal cardiac fibroblasts (RNCFs). (**A**) Detection of CTGF and FGF2 protein expression in the mixture of supernatant and eluted extracellular matrix of RNCFs, stimulated by 10 ng/ml TGF-β1 for 24 hours, with or without 2.5 μM Y27632. Ponceau S staining of the membrane shows equal loading. (**B**) ELISA quantification of FGF2 concentration in eluted extracellular matrix of RNCFs, stimulated by TGF-β1 with or without Y27632 (n = 6–9, each in triplicate). $^{**}P < 0.01$ vs. vehicle-stimulated RNCFs. $^{\#\#}P < 0.01$ vs. TGF-β1-stimulated RNCFs without Y27632. (**C**) Detection of CTGF and FGF2 protein expression in the mixture of supernatant and eluted extracellular matrix of TGF-β1–stimulated RNCFs, transfected with control, ROCK1, or ROCK2 siRNA. (**D**) ELISA quantification FGF2 concentration in eluted extracellular matrix of TGF-β1–stimulated RNCFs, transfected with control, ROCK1, or ROCK2 siRNA (n = 5–8, each in triplicate). $^{**}P < 0.01$ vs. vehicle-stimulated RNCFs transfected with each siRNA. $^{\#\#}P < 0.01$ vs. TGF-β1–stimulated RNCFs transfected with control siRNA. $^{\dagger}P < 0.05$ vs. TGF-β1–stimulated RNCFs transfected with ROCK1 siRNA. Data are expressed as mean ± SEM. (**E** and **F**) Representative fluorescent images and quantification of cellular hypertrophy of rat H9C2 cardiomyocytes stained with sarcomeric α-actinin (green), in response to 0–100 ng/ml FGF2 for 24 hours. Nuclei are stained with DAPI (blue). (n = 30–50 each). Scale bars: 25 μm. (**G–I**) Quantification of RT-PCR analysis of hypertrophic markers of Acta1 (encoding skeletal muscle α-actin), Myh7 (β-myosin heavy chain), and Nppa (atrial natriuretic factor) in H9C2 cells stimulated by FGF2 (n = 3–4 each). $^{*}P < 0.05$, $^{**}P < 0.01$ vs. vehicle-stimulated H9C2 cells. Data are expressed as mean ± SEM. P values were calculated using one-way ANOVA with Tukey's HSD test.

Methods

Generation of fibroblast-specific ROCK2-deficient mice. Conditional *Rock2*$^{flox/flox}$ mice were generated (mixed background of C57BL/6 and SV/129) as previously described (15) and were backcrossed more than 10 generations onto the C57BL/6 background. Exon 3 of the mouse *Rock2* gene was flanked by two loxP elements to generate *Rock2*$^{flox/flox}$ mice. Fibroblast-specific periostin promoter-driven Cre (*Postn*-Cre) transgenic mice (mixed background) were provided by Simon J. Conway (Indiana University School of Medicine, Indianapolis, Indiana, USA). Cre recombinase was driven by a 3.9-kb mouse *Postn* promoter (44–46). To obtain a fibroblast-specific deletion of the *Rock2* gene, *Rock2*$^{flox/flox}$ mice were crossed to *Postn*-Cre transgenic mice. The resulting *Postn*-Cre$^{+/-}$/*Rock2*$^{flox/flox}$ (ROCK2$^{Postn-/-}$) were used for all experiments. *Postn*-Cre$^{-/-}$/*Rock2*$^{flox/flox}$ (ROCK2$^{flox/flox}$) were used as littermate controls. Male ROCK2$^{Postn-/-}$ and the littermate ROCK2$^{flox/flox}$ mice at 8–10 weeks old were used in the present study. The primers used to genotype transgenic mice are as follows: *Postn* promoter Cre, 5′-CATTTGGGCCAGCTAAACAT-3′ and 5′-CCCGGCAAAACAGGTAGTTA-3′; LoxP *Rock2*, 5′-CCAGAAGACTTTAGTAAGCT-3′, and 5′-GGCAACTCCAAAATAAAGGA-3′. Animals were housed in a specific pathogen-free facility maintained by the University of Chicago Animal Resources Center.

Generation of fibroblast-specific constitutive-active knock-in ROCK mice. Conditional constitutive-active human *ROCK*-floxed (ca*ROCK*$^{flox/flox}$) mice were provided by Farhad R. Danesh (Baylor College of Medicine, Houston,

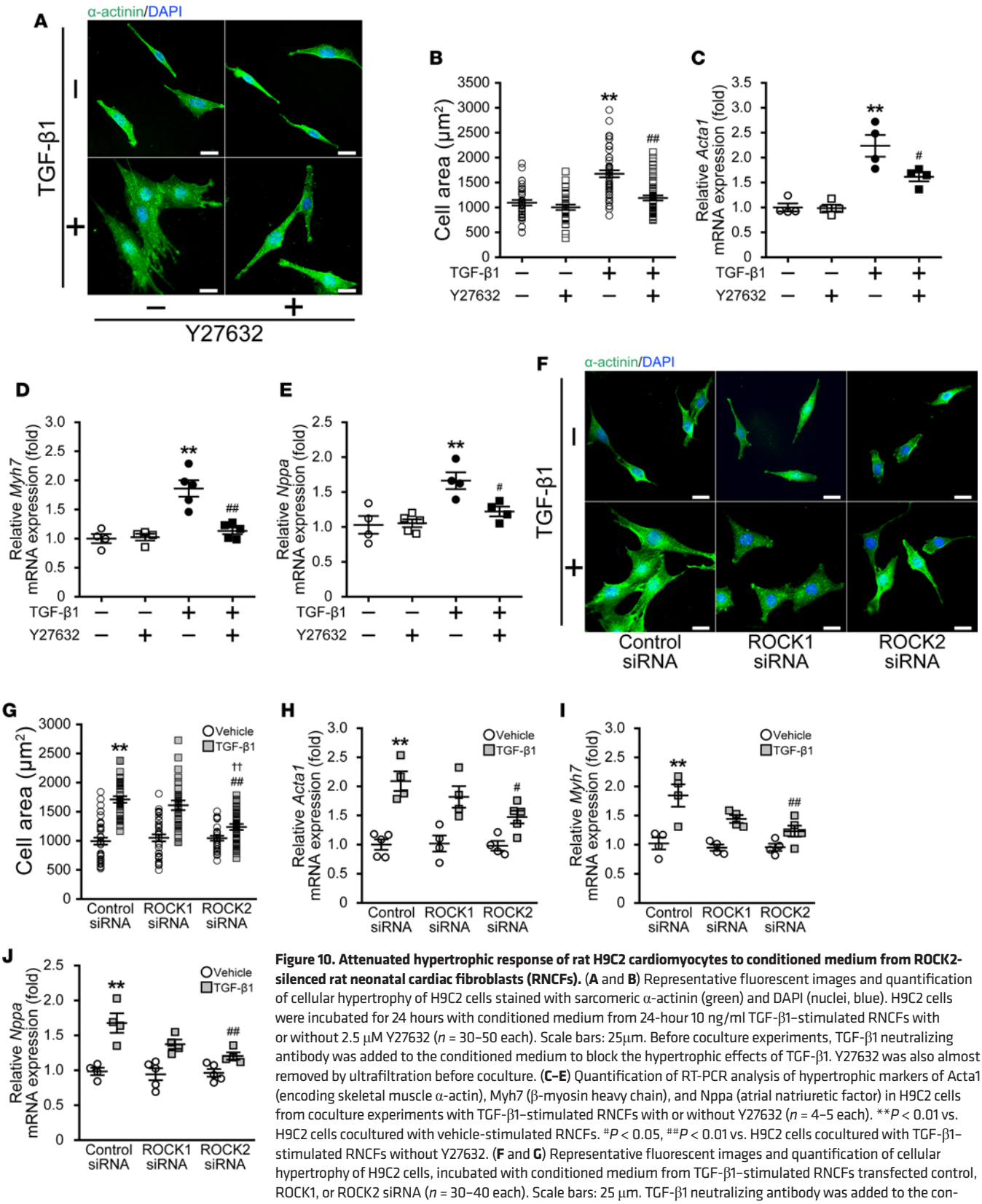

Figure 10. Attenuated hypertrophic response of rat H9C2 cardiomyocytes to conditioned medium from ROCK2-silenced rat neonatal cardiac fibroblasts (RNCFs). (**A** and **B**) Representative fluorescent images and quantification of cellular hypertrophy of H9C2 cells stained with sarcomeric α-actinin (green) and DAPI (nuclei, blue). H9C2 cells were incubated for 24 hours with conditioned medium from 24-hour 10 ng/ml TGF-β1–stimulated RNCFs with or without 2.5 μM Y27632 (n = 30–50 each). Scale bars: 25μm. Before coculture experiments, TGF-β1 neutralizing antibody was added to the conditioned medium to block the hypertrophic effects of TGF-β1. Y27632 was also almost removed by ultrafiltration before coculture. (**C–E**) Quantification of RT-PCR analysis of hypertrophic markers of Acta1 (encoding skeletal muscle α-actin), Myh7 (β-myosin heavy chain), and Nppa (atrial natriuretic factor) in H9C2 cells from coculture experiments with TGF-β1–stimulated RNCFs with or without Y27632 (n = 4–5 each). $^{**}P < 0.01$ vs. H9C2 cells cocultured with vehicle-stimulated RNCFs. $^{\#}P < 0.05$, $^{\#\#}P < 0.01$ vs. H9C2 cells cocultured with TGF-β1–stimulated RNCFs without Y27632. (**F** and **G**) Representative fluorescent images and quantification of cellular hypertrophy of H9C2 cells, incubated with conditioned medium from TGF-β1–stimulated RNCFs transfected control, ROCK1, or ROCK2 siRNA (n = 30–40 each). Scale bars: 25 μm. TGF-β1 neutralizing antibody was added to the conditioned medium before coculture. (**H–J**) Quantification of RT-PCR analysis of hypertrophic markers of Acta1, Myh7, and Nppa in H9C2 cells from coculture experiments with TGF-β1–stimulated RNCFs transfected with control, ROCK1, or ROCK2 siRNA (n = 4–5 each). $^{**}P < 0.01$ vs. H9C2 cells cocultured with vehicle-stimulated RNCFs transfected with control siRNA. $^{\#\#}P < 0.01$ vs. H9C2 cells cocultured with TGF-β1–stimulated RNCFs transfected with control siRNA. $^{\dagger\dagger}P < 0.01$ vs. H9C2 cells cocultured with TGF-β1–stimulated RNCFs transfected with ROCK1 siRNA. Data are expressed as mean ± SEM. P values were calculated using one-way ANOVA with Tukey's HSD test.

Texas, USA). The ca*ROCK* construct containing the amino-terminal kinase domain of human *ROCK1* under the control of ubiquitin-C (UbiC) promoter, which was deactivated by loxP-Stop-loxP cassettes, was inserted into the murine ubiquitous Rosa-26 locus (47). Overexpression of the ROCK1 kinase domain would be expected to activate downstream effects of both ROCK1 and ROCK2, thus termed caROCK. The ca*ROCK*$^{flox/flox}$ mice were backcrossed more than 10 generations onto C57BL/6 background. To obtain a fibroblast-specific constitutively active *ROCK* gene, the ca*ROCK*$^{flox/flox}$ mice were crossed with *Postn*-Cre transgenic mice, which resulted in the generation of mice with genotypes of *Postn*-Cre$^{+/-}$/ca*ROCK*$^{flox/flox}$ (caROCK$^{Postn-/-}$). caROCK$^{flox/flox}$ mice were used as littermate controls. The primers used to genotype ca*ROCK*$^{flox/flox}$ are as follows: Rosa-26, 5′-AATACCTTTCTGGGAGTTCT-3′ and 5′-TGAGCATGTCTTTAATCTAC-3′; UbiC (reverse), 5′-CTAAGGCCGAGTCTTATGAGCA-3′.

Ang II Infusion. Eight- to 10-week-old ROCK2$^{Postn-/-}$ and caROCK$^{Postn-/-}$ mice, and their age-matched littermate control mice, were implanted with mini-osmotic pumps (ALZET model 2004; Durect Corp) containing Ang II (A9525; Sigma-Aldrich; 1,000 ng/kg/min) or vehicle (saline) for 4 weeks to induce cardiac fibrosis and hypertrophy, as previously described (15). Briefly, a 1.0-cm vertical midscapular skin incision was made in mice anesthetized with isoflurane, followed by a creation of a 3.5-cm deep pocket, where a miniosmotic pump was inserted. Skin closure was performed using 4-0 silk sutures, and mice were allowed to recover on a heating plate at 37°C.

Blood pressure. Four weeks after the implantation of the miniosmotic pump, blood pressure and heart rate were measured by noninvasive tail-cuff method (BP-2000; Visitech Systems Inc.) on a preheated 37°C plate to dilate the tail artery, as previously described (15). The average of no less than 10 successive measurements for each mouse was taken as the individual blood pressure and heart rate values.

Echocardiography. Transthoracic echocardiography was performed with a high-resolution microimaging system equipped with a 30-MHz transducer (Vevo2100; VisualSonics Inc.), as previously described (15). After isoflurane inhalation, heart rate was adjusted to 450–550 beats/min in each group by adjusting the concentration of isoflurane. Then, cardiac echocardiography was recorded on a heating plate at 37°C. To evaluate the precise cardiac function, these adjustments of both heart rate and body temperature in each group were made. M-mode cardiac images of the LV from the short-axis view were used to assess LV morphological parameters; end-systolic IVS, end-diastolic LV PW thickness, LVDd and LVDs, and LV mass, as well as LV systolic parameters; EF and FS. LV mass, EF, and FS were calculated as follows: $1.053 \times ([LVDd + PW + IVS]^3 - [LVDd]^3)$ (mg), $100 \times ([LVEDV - LVESV]/LVEDV)$ (%), and $100 \times ([LVDd - LVDs]/LVDd)$ (%). Pulse-wave Doppler images of mitral inflow from the apical 4-chamber view were used to assess LV diastolic parameters; transmitral E/A ratio, transmitral E-wave deceleration time (DT), LV IVRT, and corrected IVRT (%IVRT), which was normalized to each R-wave and R-wave interval and expressed as a percentage of the cardiac cycle.

Western blotting. Protein was extracted from tissues or cells as previously described (48). The same amount of extracted protein was loaded on SDS-PAGE gel and transferred to PVDF membranes (Immobilon-P; Millipore). The membranes were stained in Ponceau S dye (P7170; Sigma-Aldrich) briefly to examine equal protein loading and transfer. The membranes were blocked with 3% BSA (A7906; Sigma-Aldrich) and 0.1% Tween-20 (B1379; Sigma-Aldrich) in TBS for 1 hour at room temperature and then immunoblotted by incubation overnight at 4°C with anti-ROCK1 (sc-5560; Santa Cruz Biotechnology Inc.), anti-ROCK1 (611136; BD Biosciences), anti-ROCK2 (sc-5561; Santa Cruz Biotechnology Inc.), anti-ROCK2 (610623; BD Biosciences), anti–myosin binding subunit (anti-MBS) (612164; BD Biosciences), anti–phospho-MBS (Thr853) (36-003; Millipore), anti-FGF2 (05-118; Millipore), anti-CTGF (sc-365970; Santa Cruz Biotechnology Inc.), anti–α-SMA (ab5694; Abcam), anti–β-MHC (sc-53090; Santa Cruz Biotechnology Inc.), anti-ANF (sc-20158; Santa Cruz Biotechnology Inc.), anti–collagen I (sc-8784; Santa Cruz Biotechnology Inc.), anti–cleaved caspase-3 (9661; Cell Signaling Technologies), anti–TGF-β1 (sc-146; Santa Cruz Biotechnology Inc.), anti–p38 MAPK (8690; Cell Signaling Technologies), anti–phospho-p38 MAPK (4511; Cell Signaling Technologies), anti–ERK 1/2 (9120; Cell Signaling Technologies), anti–phospho-ERK 1/2 (4370; Cell Signaling Technologies), anti-JNK (9252; Cell Signaling Technologies), anti–phospho-JNK (9251; Cell Signaling Technologies), and anti-GAPDH (2118; Cell Signaling Technologies) antibodies. The regions containing proteins were visualized by the enhanced chemiluminescence kit (Clarity Western ECL Substrate; Bio-Rad) as previously described (49). Densitometric analysis was performed using Image J Software (NIH). Densitometric readings of band intensities were normalized to GAPDH expression level.

RNA isolation and quantitative PCR. Total RNA was extracted from cells and tissues, using the PureLink RNA Mini Kit (Invitrogen) and the RNeasy Fibrous Tissue Mini Kit (Qiagen), respectively, according to the manufacturer instructions. Total RNA was converted to cDNA using the iScript Reverse Transcription Supermix Kit (Bio-Rad). The iTaq Universal SYBR Green Supermix (Bio-Rad) was used to perform amplifications in triplicate with the two-step protocol on the StepOnePlus Real-Time PCR System (Applied Biosystems). The Ct value calculated by the StepOne Software version 2.3 (Applied Biosystems) for all samples was normalized with the housekeeping gene glyceraldehyde-3-phosphate dehydrogenase. The relative fold change was computed by the ΔΔCt method. Quantitative PCR (qPCR) was performed in triplicate for each gene. The following primers were used: murine *Gapdh* (glyceraldehyde-3-phosphate dehydrogenase; forward: 5′-GGCAAATTCAACGGCACAGT-3′, reverse: 5′-CGCTCCTGGAAGATGGTGAT-3′); murine *Rock1* (forward: 5′-GAGTCCCTGAACAGAGAATTAC-3′, reverse: 5′-TTCGCTCAGCTTCCAATAC-3′); murine *Rock2* (forward: 5′-AGGTACGACTTGGAAGAAATG-3′, reverse: 5′-CTGCCGTCTCTCT-TATGTTATC-3′); murine *Ctgf* (connective tissue growth factor; forward: 5′-AACTATGATGCGAGC-CAAC-3′, reverse: 5′-CCAGTCTGCAGAAGGTATTG-3′); murine *Fgf2* (forward: 5′-CCCACACGT-CAAACTACAA-3′, reverse: 5′-CGTCCATCTTCCTTCATAGC-3′); murine *Acta1* (skeletal muscle α-actin; forward: 5′-CTGGACTTCGAGAATGAGATG-3′, reverse: 5′-GATAAAGGAAGGCTGGAAGAG-3′); murine *Acta2* (α-SMA; forward: 5′-GACTCACAACGTGCCTATC-3′, reverse: 5′-GCAGTAGTCAC-GAAGGAATAG-3′); murine *Fn1* (fibronectin 1; forward: 5′-AGAAGGCAGTAGCACAGA-3′, reverse: 5′-TCTCCTCCACAGCATAGATAG-3′); murine *Nppa* (ANF; forward: 5′-GAAGATGCCGGTAGAA-GATG-3′, reverse: 5′-CTCTCAGAGGTGGGTTGA-3′); murine *Col1a* (collagen type I α 1; forward: 5′-CAATGGTGCTCCTGGTATTG-3′, reverse: 5′-CACCAGTGTCTCCTTTGTTG-3′); murine *Tgfb1* (transforming growth factor-β1; forward: 5′- GAAGCGGACTACTATGCTAAAG-3′, reverse: 5′- CCC-GAATGTCTGACGTATTG-3′); rat *Gapdh* (forward: 5′-CTCCCATTCTTCCACCTTTG-3′, reverse: 5′-CCTGTTGCTGTAGCCATATT-3′); rat *Rock1* (forward: 5′-TCCTACCCTCTACCACTTTC-3′, reverse: 5′-TCCCTGTGGGACTTAACA-3′); rat *Rock2* (forward: 5′-GGAGTTCCAACTGCTGTATC-3′, reverse: 5′-TCCCTGTGGGACTTAACA-3′); rat *Acta1* (forward: 5′-GCCCATCTATGAGGGTTATG-3′, reverse: 5′-CTGTGGTCACGAAGGAATAG-3′); rat *Nppa* (forward: 5′-AGGCCATATTGGAGCAAATC-3′, reverse: 5′-AGGCATGACCTCATCTTCTA-3′); and rat *Myh7* (β-myosin heavy chain; forward: 5′-TGGCAC-CGTGGACTACAATA-3′, reverse: 5′-TACAGGTGCATCAGCTCCAG-3′).

Histological assessment of cardiac interstitial fibrosis. Mouse heart samples were isolated, fixed with 10% formaldehyde in PBS at room temperature for 24 hours, embedded in paraffin, and sectioned at 5 μm. Picrosirius red stain kit (Polysciences Inc.) was performed to identify collagen fibers, following manufacturer's instructions. Picrosirius red-stained interstitial fibrosis was observed under the light microscopy (BX 41, Olympus) at ×20 magnification. The digital photomicrographs were quantified with Image J (NIH). The percent area of extracellular Picrosirius red staining was computed from five random fields within the mid-myocardium in each murine sample, in order to exclude large epicardial arteries/veins and any cutting/compression artifacts.

Histological assessment of cardiac hypertrophy. Formalin-fixed paraffin sections of the mouse heart were stained with Texas Red-X-conjugated wheat germ agglutinin (WGA) (W21405; Invitrogen) to evaluate myofiber size. WGA-stained cell membrane was observed under the fluorescence microscopy (BX41, Olympus) at ×40 magnification. One-hundred to 200 cells for each mouse sample were measured using Image J (NIH) to determine the cross-sectional area of cardiomyocyte.

Double immunostaining of ROCK2 and periostin. Mouse heart samples were isolated, fixed in fresh 4% paraformaldehyde in PBS at 4°C for 6 hours, embedded in OCT compound (Tissue-Tek, Sakura Fine-tek), snap-frozen, and sectioned at 8 μm. After blocking with 3% BSA in PBS for 1 hour, cryosections were immunostained with primary antibodies against rabbit polyclonal ROCK2 (sc-5561; Santa Cruz Biotechnology Inc.) and goat polyclonal periostin (sc-49480; Santa Cruz Biotechnology Inc.), visualized with secondary antibodies conjugated with Alexa Fluor 488 and 594 (A21206 and A11058; Invitrogen), respectively. Negative control experiments were performed with the isotype-matched IgG (sc-2027 and sc-2028; Santa Cruz Biotechnology Inc.). Finally, coverslips were mounted with Prolong Gold Antifade Reagent with DAPI (P-36391; Invitrogen) to fluorescently label nuclei blue. Fluorescent images were obtained by laser scanning confocal microscopy (FV1000, Olympus).

Harvesting of mouse CFs. Adult CFs were isolated from cardiac ventricles of 12- to 14-week-old ROCK2$^{Postn-/-}$ and caROCK$^{Postn-/-}$ mice and their littermate control mice after Ang II and saline

treatment. Five mice were used for each preparation. The mice were sacrificed by cervical dislocation following CO_2 overdose. The heart samples were quickly excised under sterile conditions, rinsed in HBSS (Invitrogen), thoroughly minced to 1- to 2-mm pieces, and digested with 200 U/ml type II collagenase (Worthington Biochemical) in Dulbecco's phosphate-buffer saline (DPBS, Invitrogen) at 37°C for 15 minutes by constant stirring. After undigested heart tissues were allowed to settle, the supernatant from the first digestion, containing large amounts of cell debris and blood cells, was discard. At the end of the subsequent second digestion by type II collagenase, the supernatant, composed of mostly CFs, was carefully aspirated, transferred to a fresh tube, centrifuge at 250 *g* for 5 minutes, and resuspended in DMEM with 10% FBS and 1% penicillin/streptomycin (P/S, Invitrogen). This digestion was repeated 6-8 times in the same way until the digestion solution became clear. Cells were plated on gelatin-coated 60-mm dishes. After incubation for 2 hours at 37°C, allowing CFs to attach to the bottom of plate, unattached cells, including primary myocytes, endothelial cells, and leukocytes, were washed away. CFs were cultured in DMEM with 10% FBS and 1% P/S at 37°C in a humidified atmosphere of 5% CO_2 and 95% air. The CFs at passage 2–3 at 70%–80% confluence were used for all experiments.

Isolation and immortalization of MEFs. Primary MEFs were cultured from 13-day-old embryos, derived by intercrosses of WT, global heterozygous *Rock1*-KO (ROCK1$^{+/-}$), and global heterozygous *Rock2*-KO (ROCK2$^{+/-}$) mice, all of which were on the C57BL/6 background. The embryos were separated from their yolk sac and placed in the complete growth medium, DMEM with 10% FBS, 1% P/S, and 1% GlutaMAX (Invitrogen). After the embryonic head and innards were removed, the body was homogenized and trypsinized at 37°C for 45 min. To detect homozygous *Rock1* (ROCK1$^{-/-}$) and *Rock2* (ROCK2$^{-/-}$) deletion, genotyping by PCR was performed with genomic DNA isolated from the embryonic head, as previously described (14, 15). After quenching the trypsin with the complete growth medium, the MEFs were isolated from the remaining embryonic body by repeated pipetting and cultured until confluent. After the third passage, the MEFs from each strain were immortalized by infection with a retrovirus vector expressing SV40 large T antigen, using neomycin selection for 2 weeks. MEFs for experimental use were cultured in gelatin-coated dishes. After serum starvation overnight, MEFs were pretreated with or without 10 μM ROCK inhibitor Y27632 (688001; Millipore) for 1 hour and then stimulated for 24 hours with 1 μM Ang II (A9525; Sigma-Aldrich) or 10 ng/ml TGF-β1 (100-21C; PeproTech).

Transfection of RNCFs with siRNA. RNCFs were purchased from ScienCell Research Laboratories (R6330) and cultured at 37 °C and 5% CO_2 in Fibroblast Medium-2 (2331; ScienCell) containing 5% FBS, Fibroblast Growth Supplement-2 (2382; ScienCell), and 1% P/S. Cells used for all experiments were passaged between 2–5 times. All siRNA and transfection reagents were purchased from Invitrogen and were used according to the manufacturer's instructions. Briefly, RNCFs were seeded at subconfluent densities in gelatin-coated 6-well plates or 100-mm culture dishes in DMEM containing 10% FBS without antibiotics for 24 hours before transfection. Silencer Select Negative Control No. 1 (4390843) or Silencer Cy3-labeled Negative Control No. 1 (AM4621) were used as a control (control siRNA). ROCK1 siRNA (s135694), ROCK2 siRNA (s130059), and control siRNA were diluted to 10 nM in Opti-MEM (31985070). Lipofectamine RNAiMax (13778075) was also mixed with Opti-MEM and incubated at room temperature for 20 minutes. This siRNA-lipid mixture were added to RNCFs and incubated to perform transfection. At 48 hours after transfection, RNCFs were harvested to determine the expression of ROCK1 and ROCK2 protein and mRNA using Western blotting and qPCR analyses, respectively.

Measurement of FGF2-induced cardiac hypertrophy in rat H9C2 cardiomyocytes. Rat H9C2 cardiomyocytes were purchased from the American Type Culture Collection (ATCC; CRL-1466) and cultured at 37°C and 5% CO_2 in DMEM containing 10% FBS and 1% P/S. Cells used for all experiments were passaged between 2–5 times. H9C2 cells for experimental use were seeded at 5,000/cm^2 in gelatin-coated 6-well plates or chamber slides. After serum-starvation overnight, H9C2 cells were treated for 24 hours with 0-100 ng/ml FGF2 (100-18B; PeproTech). For immunocytochemical analysis, H9C2 cells in chamber slides were fixed, permeabilized, blocked, incubated with primary antibody against mouse monoclonal sarcomeric α-actinin (A7811; Sigma-Aldrich), visualized with secondary antibody conjugated with Alexa Fluor 488 (A11001; Invitrogen), and finally mounted with Prolong Gold Antifade Reagent with DAPI (P-36391; Invitrogen). Quantification of H9C2 cell-surface area was performed on α-actinin-stained cells using the fluorescence microscopy (BX41, Olympus) at ×40 magnification and Image J (NIH) and calculated as the mean of at least 40 cells in random 15–20 fields. The mRNA expression of prohypertrophic markers of H9C2 cells in 6-well plates were analyzed by qPCR.

Quantification of intracellular and extracellular FGF2 from RNCFs. RNCFs without siRNA transfection were seeded for 24 hours at subconfluent densities in 6-well plates containing DMEM with 10% FBS and 1% P/S, followed by overnight serum starvation and 1-hour pretreatment with 2.5 or 10 μM Y27632 (688001; Millipore), while RNCFs, following 48-hour transfection with ROCK1 or ROCK2 siRNA, were serum starved overnight. These cells were stimulated for 24 hours with 10 ng/ml TGF-β1 (100-21C; PeproTech) in 1 ml DMEM. To release and harvest extracellular FGF2, after removal of supernatant, RNCFs were gently washed with DMEM and then incubated for 10 minutes with 0.25 ml of NaCl buffer (2 M NaCl and 10 mM Tris HCl, pH 7.2) containing 0.5% BSA (50). This NaCl wash buffer was collected and filtered through a 0.22-μm filter to remove cell debris. FGF2 protein in this NaCl wash buffer was quantitated using rat FGF2 ELISA kit according to manufacturer's instructions (MFB00; R&D Systems). In addition, the mixture of both supernatant and subsequent NaCl wash buffer was filtered and concentrated 100-fold using a 10 kDa cut-off filter (Amicon Ultra-10; Millipore). FGF2 protein in this mixture was detected by Western blotting analysis. To detect intracellular FGF2, the remaining RNCFs were gently washed in DMEM and then lysed with cell lysis buffer as previously described (48). The expression of proteins including FGF2 were analyzed by Western blotting.

Assessing ROCK activity and diastolic function in patients. Patients with HFpEF were screened using systematic data query of inpatient electronic medical records at University of Chicago using the following search criteria: diagnosis of HF, B-type natriuretic peptide (BNP) > 100 pg/ml, or administration of two or more doses of i.v. diuretics. Medical records were then examined, and patients were enrolled in the study if they met the following criteria: age ≥ 21 years, LV ejection fraction (LVEF) ≥ 50%, and presence of HF as defined by Framingham Criteria (51). Patients with moderate or severe valvular heart disease, cardiac transplantation, previously reduced LVEF (<35%) that had normalized, and infiltrative or genetic cardiomyopathies were excluded. Age- and sex-matched controls were found for a subset of the patients with diastolic dysfunction using systematic data query of outpatient visits at the University of Chicago Primary Care Group clinic, and were considered if they were in general good health, and excluded if they had active acute medical conditions, symptoms of HF or angina, uncontrolled hypertension or diabetes, known coronary artery disease, known HF, moderate or severe lung disease, malignancies, or more than 2 chronic medical conditions including hypertension, diabetes, and coronary artery disease. These patients underwent screening 2-dimensional echocardiography to confirm normal LVEF and normal LV thickness and to exclude significant valvular heart disease. Full transthoracic echocardiography was performed on all patients, and measurements were made by a single investigator blinded to the ROCK activity.

Diastolic dysfunction parameters measured included pulse-wave mitral inflow Doppler, tissue Doppler of the mitral annulus, left atrial (LA) volume, and tricuspid regurgitation jet velocity. In the apical four-chamber view, the pulsed-wave Doppler sample volume was targeted at the tips of the mitral valve to assess peak early (E) and late (A) diastolic transmitral filling velocities. In the same view, peak early diastolic mitral annular tissue velocities (e') were obtained by placing the pulsed-wave tissue Doppler sample volume on both the lateral and septal mitral annulus and recorded using pulsed-wave Doppler. In a modified apical 4-chamber view, tricuspid regurgitation velocity was measured using continuous-wave velocity directed through the center of the tricuspid valve leaflets. LA volume was measured using the biplane area-length (ellipsoid) method (52). Diastolic dysfunction grade was determined using current American Society of Echocardiography guidelines, which incorporates several diastolic function parameters to assign a grade of 0-3 (53).

Leukocytes were isolated from 10 ml peripheral blood obtained from patients, frozen and stored at -80 °C until 10 or more samples were collected. ROCK assays were performed on batched samples. The samples underwent sodium dodecyl sulfate-polyacrylamide gel electrophoresis, and bound proteins were detected by immunoblotting (49).

Conditioned medium from RNCFs and coculture with H9C2 cells. After treatment with 2.5 μM Y27632 or transfection with ROCK1 or ROCK2 siRNA, RNCFs in 100-mm culture dishes were serum starved and stimulated for 24 hours with 10 ng/ml TGF-β1. The mixture of supernatant in DMEM and subsequent NaCl wash buffer was collected, filtered, and treated with 30 μg/ml neutralizing anti-TGF-β1 antibody (MAB240; R&D Systems). After neutralizing TGF-β1, the mixture medium was concentrated 100-fold, desalted, and dialyzed in DMEM using Amicon Ultra-15 repeatedly over 8 times to remove almost all of both NaCl and Y27632. H9C2 cells in gelatin-coated 24-well or chamber slides were serum starved and then cocultured for 24 hours in 1:1 mixed medium of serum-free DMEM and the concentrated conditioned medium from RNCFs.

Statistics. All data are expressed as the mean ± SEM. Comparisons of parameters were performed with the unpaired Student's *t* test or ANOVA followed by post hoc Tukey's HSD test for multiple comparisons. Comparison of ROCK activity in patients with diastolic dysfunction versus control patients was performed using paired *t* test analysis. In addition, median and interquartile range of ROCK activity was determined in all 3 diastolic dysfunction grades. Statistical significance was evaluated with JMP 11 (SAS Institute Inc.). A *P* value of less than 0.05 was considered to be statistically significant.

Study approval. All animal protocols were approved by the Institutional Animal Care and Use Committee (IACUC) of the University of Chicago. Studies performed using leukocytes from patients with diastolic dysfunction were approved by the IRB of the University of Chicago (IRB protocol numbers: 12-0927 and 14-0316), and prior to participation, written informed consent was obtained from each subject.

Author contributions

The following contributions were made by the authors:

TS: Designed and performed most of the studies; analyzed results, prepare figures and tables, and wrote initial drafts of manuscript. NN: Performed and analyzed echocardiograms in patients. PC: Isolated and immortalized MEFs from wild-type, global *Rock1* knockout, and global *Rock2* knockout mice. BY: Performed leukocyte ROCK assays. MK: Isolated peripheral leukocytes from patients and helped performed ROCK assays. JJ: Isolated peripheral leukocytes from patients; helped with mouse breeding and genotyping. JB: Designed, recruited, and performed echocardiographic studies on patients with diastolic dysfunction and controls; wrote the clinical portion of the manuscript. JKL: Conceived, designed, and coordinated the entire study; wrote final version of manuscript.

Acknowledgments

This work was supported by grants from the NIH (HL052233, NS070001, DK085006). We thank Simon Conway (Indiana University School of Medicine) and Farhad R. Danesh (Baylor College of Medicine) for providing Postn-Cre and caROCK$^{flox/flox}$ mice, respectively.

Address correspondence to: James K. Liao, Section of Cardiology, Department of Medicine, University of Chicago, 5841 S. Maryland Avenue, MC 6080, Chicago, Illinois 60637, USA. Phone: 773.702.8950; Email: jliao@medicine.bsd.uchicago.edu.

1. Go AS, et al. Heart disease and stroke statistics--2013 update: a report from the American Heart Association. *Circulation*. 2013;127(1):e6–e245.
2. Lee WC, Chavez YE, Baker T, Luce BR. Economic burden of heart failure: a summary of recent literature. *Heart Lung*. 2004;33(6):362–371.
3. Owan TE, Hodge DO, Herges RM, Jacobsen SJ, Roger VL, Redfield MM. Trends in prevalence and outcome of heart failure with preserved ejection fraction. *N Engl J Med*. 2006;355(3):251–259.
4. Steinberg BA, et al. Trends in patients hospitalized with heart failure and preserved left ventricular ejection fraction: prevalence, therapies, and outcomes. *Circulation*. 2012;126(1):65–75.
5. Bhatia RS, et al. Outcome of heart failure with preserved ejection fraction in a population-based study. *N Engl J Med*. 2006;355(3):260–269.
6. SOLVD Investigators, Yusuf S, Pitt B, Davis CE, Hood WB, Cohn JN. Effect of enalapril on mortality and the development of heart failure in asymptomatic patients with reduced left ventricular ejection fractions. *N Engl J Med*. 1992;327(10):685–691.
7. Stehlik J, et al. The Registry of the International Society for Heart and Lung Transplantation: 29th official adult heart transplant report--2012. *J Heart Lung Transplant*. 2012;31(10):1052–1064.
8. Rose EA, et al. Long-term use of a left ventricular assist device for end-stage heart failure. *N Engl J Med*. 2001;345(20):1435–1443.
9. Borlaug BA. The pathophysiology of heart failure with preserved ejection fraction. *Nat Rev Cardiol*. 2014;11(9):507–515.
10. Shimizu T, Liao JK. Rho Kinases and Cardiac Remodeling. *Circ J*. 2016;80(7):1491–1498.
11. Sawada N, Liao JK. Rho/Rho-associated coiled-coil forming kinase pathway as therapeutic targets for statins in atherosclerosis. *Antioxid Redox Signal*. 2014;20(8):1251–1267.
12. Shimokawa H, Satoh K. 2015 ATVB Plenary Lecture: translational research on rho-kinase in cardiovascular medicine. *Arterioscler Thromb Vasc Biol*. 2015;35(8):1756–1769.
13. Zhang YM, et al. Targeted deletion of ROCK1 protects the heart against pressure overload by inhibiting reactive fibrosis. *FASEB J*. 2006;20(7):916–925.
14. Rikitake Y, et al. Decreased perivascular fibrosis but not cardiac hypertrophy in ROCK1+/- haploinsufficient mice. *Circulation*. 2005;112(19):2959–2965.
15. Okamoto R, et al. FHL2 prevents cardiac hypertrophy in mice with cardiac-specific deletion of ROCK2. *FASEB J*. 2013;27(4):1439–1449.
16. Frieler RA, Mortensen RM. Immune cell and other noncardiomyocyte regulation of cardiac hypertrophy and remodeling. *Circu-*

lation. 2015;131(11):1019–1030.
17. Leask A. Getting to the heart of the matter: new insights into cardiac fibrosis. *Circ Res*. 2015;116(7):1269–1276.
18. Fujiu K, Nagai R. Fibroblast-mediated pathways in cardiac hypertrophy. *J Mol Cell Cardiol*. 2014;70:64–73.
19. Thumkeo D, et al. Targeted disruption of the mouse rho-associated kinase 2 gene results in intrauterine growth retardation and fetal death. *Mol Cell Biol*. 2003;23(14):5043–5055.
20. Lajiness JD, Conway SJ. Origin, development, and differentiation of cardiac fibroblasts. *J Mol Cell Cardiol*. 2014;70:2–8.
21. Oka T, et al. Genetic manipulation of periostin expression reveals a role in cardiac hypertrophy and ventricular remodeling. *Circ Res*. 2007;101(3):313–321.
22. Snider P, et al. Periostin is required for maturation and extracellular matrix stabilization of noncardiomyocyte lineages of the heart. *Circ Res*. 2008;102(7):752–760.
23. Kong P, Christia P, Saxena A, Su Y, Frangogiannis NG. Lack of specificity of fibroblast-specific protein 1 in cardiac remodeling and fibrosis. *Am J Physiol Heart Circ Physiol*. 2013;305(9):H1363–H1372.
24. Vliegen HW, van der Laarse A, Cornelisse CJ, Eulderink F. Myocardial changes in pressure overload-induced left ventricular hypertrophy. A study on tissue composition, polyploidization and multinucleation. *Eur Heart J*. 1991;12(4):488–494.
25. Dobaczewski M, Chen W, Frangogiannis NG. Transforming growth factor (TGF)-β signaling in cardiac remodeling. *J Mol Cell Cardiol*. 2011;51(4):600–606.
26. Mohammed SF, et al. Comorbidity and ventricular and vascular structure and function in heart failure with preserved ejection fraction: a community-based study. *Circ Heart Fail*. 2012;5(6):710–719.
27. Shi J, Wei L. Rho kinases in cardiovascular physiology and pathophysiology: the effect of fasudil. *J Cardiovasc Pharmacol*. 2013;62(4):341–354.
28. Loirand G. Rho Kinases in Health and Disease: From Basic Science to Translational Research. *Pharmacol Rev*. 2015;67(4):1074–1095.
29. Westermann D, et al. Cardiac inflammation contributes to changes in the extracellular matrix in patients with heart failure and normal ejection fraction. *Circ Heart Fail*. 2011;4(1):44–52.
30. Campbell SE, Katwa LC. Angiotensin II stimulated expression of transforming growth factor-beta1 in cardiac fibroblasts and myofibroblasts. *J Mol Cell Cardiol*. 1997;29(7):1947–1958.
31. Gray MO, Long CS, Kalinyak JE, Li HT, Karliner JS. Angiotensin II stimulates cardiac myocyte hypertrophy via paracrine release of TGF-beta 1 and endothelin-1 from fibroblasts. *Cardiovasc Res*. 1998;40(2):352–363.
32. Schultz Jel J, et al. TGF-beta1 mediates the hypertrophic cardiomyocyte growth induced by angiotensin II. *J Clin Invest*. 2002;109(6):787–796.
33. Abreu JG, Ketpura NI, Reversade B, De Robertis EM. Connective-tissue growth factor (CTGF) modulates cell signalling by BMP and TGF-beta. *Nat Cell Biol*. 2002;4(8):599–604.
34. Chen MM, Lam A, Abraham JA, Schreiner GF, Joly AH. CTGF expression is induced by TGF- beta in cardiac fibroblasts and cardiac myocytes: a potential role in heart fibrosis. *J Mol Cell Cardiol*. 2000;32(10):1805–1819.
35. Knipe RS, Tager AM, Liao JK. The Rho kinases: critical mediators of multiple profibrotic processes and rational targets for new therapies for pulmonary fibrosis. *Pharmacol Rev*. 2015;67(1):103–117.
36. Itoh N, Ohta H. Pathophysiological roles of FGF signaling in the heart. *Front Physiol*. 2013;4:247.
37. Schultz JE, et al. Fibroblast growth factor-2 mediates pressure-induced hypertrophic response. *J Clin Invest*. 1999;104(6):709–719.
38. Pellieux C, et al. Dilated cardiomyopathy and impaired cardiac hypertrophic response to angiotensin II in mice lacking FGF-2. *J Clin Invest*. 2001;108(12):1843–1851.
39. House SL, et al. Fibroblast Growth Factor 2 Mediates Isoproterenol-induced Cardiac Hypertrophy through Activation of the Extracellular Regulated Kinase. *Mol Cell Pharmacol*. 2010;2(4):143–154.
40. Santiago JJ, et al. Preferential accumulation and export of high molecular weight FGF-2 by rat cardiac non-myocytes. *Cardiovasc Res*. 2011;89(1):139–147.
41. Matsumoto E, et al. Angiotensin II-induced cardiac hypertrophy and fibrosis are promoted in mice lacking Fgf16. *Genes Cells*. 2013;18(7):544–553.
42. Nakagawa O, Fujisawa K, Ishizaki T, Saito Y, Nakao K, Narumiya S. ROCK-I and ROCK-II, two isoforms of Rho-associated coiled-coil forming protein serine/threonine kinase in mice. *FEBS Lett*. 1996;392(2):189–193.
43. Upadhya B, Taffet GE, Cheng CP, Kitzman DW. Heart failure with preserved ejection fraction in the elderly: scope of the problem. *J Mol Cell Cardiol*. 2015;83:73–87.
44. Takeda N, et al. Cardiac fibroblasts are essential for the adaptive response of the murine heart to pressure overload. *J Clin Invest*. 2010;120(1):254–265.
45. Kaur H, et al. Targeted Ablation of Periostin-Expressing Activated Fibroblasts Prevents Adverse Cardiac Remodeling in Mice. *Circ Res*. 2016;118(12):1906–1917.
46. Lal H, et al. Cardiac fibroblast glycogen synthase kinase-3β regulates ventricular remodeling and dysfunction in ischemic heart. *Circulation*. 2014;130(5):419–430.
47. Wang W, et al. Mitochondrial fission triggered by hyperglycemia is mediated by ROCK1 activation in podocytes and endothelial cells. *Cell Metab*. 2012;15(2):186–200.
48. Liu PY, Liao JK. A method for measuring Rho kinase activity in tissues and cells. *Meth Enzymol*. 2008;439:181–189.
49. Shimizu T, Fukumoto Y, Tanaka S, Satoh K, Ikeda S, Shimokawa H. Crucial role of ROCK2 in vascular smooth muscle cells for hypoxia-induced pulmonary hypertension in mice. *Arterioscler Thromb Vasc Biol*. 2013;33(12):2780–2791.
50. Khalil N, Xu YD, O'Connor R, Duronio V. Proliferation of pulmonary interstitial fibroblasts is mediated by transforming growth factor-beta1-induced release of extracellular fibroblast growth factor-2 and phosphorylation of p38 MAPK and JNK. *J Biol Chem*. 2005;280(52):43000–43009.
51. McKee PA, Castelli WP, McNamara PM, Kannel WB. The natural history of congestive heart failure: the Framingham study. *N Engl J Med*. 1971;285(26):1441–1446.
52. Lang RM, et al. Recommendations for cardiac chamber quantification by echocardiography in adults: an update from the American Society of Echocardiography and the European Association of Cardiovascular Imaging. *J Am Soc Echocardiogr*.

2015;28(1):1–39.e14.
53. Nagueh SF, et al. Recommendations for the Evaluation of Left Ventricular Diastolic Function by Echocardiography: An Update from the American Society of Echocardiography and the European Association of Cardiovascular Imaging. *Eur Heart J Cardiovasc Imaging*. 2016;17(12):1321–1360.